Precambrian Research 255 (2014) 316–334

Contents lists available at ScienceDirect

Precambrian Research

journal homepage: www.elsevier.com/locate/precamres

Silica precipitation triggered by clastic sedimentation in the Archean: New petrographic evidence from cherts of the Kromberg type section, South Africa

Morgane Ledevin[a,*], Nicholas Arndt[a], Alexandre Simionovici[a], Etienne Jaillard[a], Marc Ulrich[b]

[a] ISTerre, CNRS, F-38041 Grenoble Cedex 9, France
[b] EOST, CNRS, University of Strasbourg, 67084 Strasbourg Cedex, France

ARTICLE INFO

Article history:
Received 28 October 2013
Received in revised form
22 September 2014
Accepted 6 October 2014
Available online 25 October 2014

Keywords:
Archean
Barberton Greenstone Belt
Kromberg formation
Chert
Turbidite
Metasomatism
Siliceous ooze

ABSTRACT

The Kromberg Formation (ca. 3432 Ma) in the Barberton Greenstone Belt, South Africa, contains well-preserved chert beds at the tops of turbidite deposits. At the interface, siltstone, which consist of K-feldspar, K-mica, microquartz with minor lithic fragments and heavy minerals, grades into chert, which consists of microquartz and minor K-mica (<15%). K-feldspars show preserved twins typical of microcline, orthoclase and sanidine. Based on the heterogeneity of the clastic fraction (i.e. shape, size, nature), the lack of in situ metasomatic features (i.e. crystal overgrowths, silica replacement) and the continuity of the siliceous matrix through the siltstone-to-chert transition, we argue that (1) the clastic particles are detrital, (2) some were altered and metasomatized at their source, (3) in situ metasomatism was limited to minor seritization of K-feldspars, and (4) the silica is of primary origin and precipitated from ambient marine fluids. Our petrographic observations reinforce the model advocated by Rouchon and Orberger (2008) and Rouchon et al. (2009) for chert deposited in clastic-rich setting and we favor a formation of both the siltstones and cherts as chemico-clastic sediments. We argue for the contemporaneous deposition of clastic grains from turbiditity currents and precipitation of silica on phyllosilicate reactive surfaces, both in the water column and at the sediment–water interface. As the rate of clastic sedimentation declined, the accumulation of silica flocs on suspended phyllosilicates first accompanied, then replaced the deposition of detrital grains, to form a siliceous ooze at the seafloor. Contrary to current interpretations for detritus-rich cherts, which invoke a secondary origin via Si- and K-metasomatism, we propose that the present model prevailed in a variety of Archean settings where fine-grained sediments were deposited. The composition of both the siltstone and chert reflects mainly the environment in which they formed. They are interpreted as mixtures of two main components: (1) silica, which contains extremely low concentrations of trace elements and contributes only SiO_2 to the bulk composition, and (2) another phase that dominates the trace element composition. Here, K-mica and K-feldspar control the chemical signal and reflect a felsic source to the turbidites (i.e. Hooggenoeg dacites and volcaniclastics).

1. Introduction

On the modern Earth, ever since the Proterozoic, both the silica cycle and the formation of cherts are essentially controlled by biological activity; during the Archean, however, the absence of skeleton-forming organisms allowed only inorganic silica precipitation (e.g. Siever, 1992; Treguer et al., 1995; Perry and Lefticariu, 2003; Maliva et al., 2005). The voluminous chert deposits found in Archean greenstone belts are therefore interpreted to reflect the physico-chemical conditions of the eon, and particularly elevated concentrations of dissolved silica in the oceans (e.g. Siever, 1992; Maliva et al., 2005).

Cherts through geological time show a wide variety of depositional environments, chemical compositions, mineralogies and formation processes. There is, however, no consensus on the nomenclature, nor even on the definition, of chert. All authors agree that the silica content must exceed 75–80 wt% (e.g. Folk, 1980; Knauth, 1994), but differences emerge regarding the origin of cherts. Two models dominate the discussion: (1) silicification of preexisting rocks, or (2) direct precipitation of silica from seawater or hydrothermal fluids.

* Corresponding author. Present adress: ISTerre, BP53, 38041 Grenoble Cedex 9, France. Tel.: +33 (0)4 76 63 59 31.
E-mail address: morgane.ledevin@ujf-grenoble.fr (M. Ledevin).

http://dx.doi.org/10.1016/j.precamres.2014.10.009
0301-9268/

In the first model, Archean cherts are considered to result from the pervasive replacement of a variety of rock precursors, including (i) volcaniclastic and terrigenous debris (e.g. Lowe and Knauth, 1977; Lowe, 1980; Paris et al., 1985; De Vries, 2004), (ii) chemical sediments such as carbonates and evaporites (Knauth, 1973; Lowe and Knauth, 1977; Knauth and Lowe, 1978; Weis and Wasserburg, 1987; Lowe and Fisher Worrell, 1999; Van Kranendonk et al., 2003) and (iii) massive lavas (Hofmann and Wilson, 2007; Hofmann and Harris, 2008). The silicification is thought to be triggered either by fluid circulation during hydrothermal activity (Knauth and Lowe, 1978; de Wit et al., 1982; Duchac and Hanor, 1987; Paris et al., 1985; de Wit and Hart, 1993; Knauth, 1994; Perry and Lefticariu, 2003; Hofmann, 2005; Hofmann and Wilson, 2007; Hofmann and Harris, 2008), or by low-temperature seawater–rock interaction at or below the surface during early diagenesis (Knauth and Lowe, 1978; de Wit et al., 1982; Sugitani, 1992; Lowe, 1999; Lowe and Fisher Worrell, 1999; Van Kranendonk and Pirajno, 2004; Tice and Lowe, 2006; Rouchon and Orberger, 2008).

The second model, which invokes direct precipitation of silica from oceanic water, was first proposed for jasper layers in banded iron formations, then extended to other siliceous deposits such as banded cherts. The silica can be precipitated from Si-oversaturated seawater (Knauth and Lowe, 1978; Hesse, 1989; Sugitani et al., 1998; Perry and Lefticariu, 2003; Hofmann, 2005; Maliva et al., 2005; Tice and Lowe, 2006), from hydrothermal vent fluids near active volcanic settings (e.g. mid-oceanic ridges) (e.g. Sugitani, 1992; De Vries, 2004; Hofmann and Bolhar, 2007), or from a mixture of both (e.g. Derry and Jacobsen, 1990; Frei and Polat, 2007; Van den Boorn et al., 2007, 2010; Marin-Carbonne et al., 2012). The composition of cherts considered to have precipitated from seawater is regarded as representative of early ocean chemistry, making them among the most powerful tools to investigate early Earth environments (e.g. Derry and Jacobsen, 1990; Sugitani et al., 1996, 1998; Knauth and Lowe, 2003; Perry and Lefticariu, 2003, 2006; Kato and Nakamura, 2003; Bolhar et al., 2005; Robert and Chaussidon, 2006; Jaffres et al., 2007).

However, criteria for the recognition of the various chert types are ambiguous and none can reliably distinguish between primary oceanic precipitates, hydrothermal deposits and secondary cherts. Criteria commonly used include field relations and sedimentary structures (e.g. Knauth and Lowe, 2003; Maliva et al., 2005), petrological characteristics (e.g. Knauth, 1994; Knauth and Lowe, 2003), and trace element and/or isotopic compositions (e.g. Kato and Nakamura, 2003; Bolhar et al., 2005; Van den Boorn et al., 2007, 2010; Marin et al., 2010; Marin-Carbonne et al., 2011, 2012), the latter approach being perhaps the most popular. Identification of formation processes is especially challenging for cherts formed in clastic environments, which are made up of a detrital component and silica cement. Following accepted models, such a rock would be considered to have formed either by the precipitation of silica from marine fluids contemporaneously with clastic sedimentation, or by silica addition and replacement of primarily deposited sediments during diagenesis and secondary fluid circulation (i.e. Si-metasomatism).

For this study we chose the Kromberg type section (ca. 3432 Ma) in the Barberton Greenstone Belt, South Africa, because it contains well-preserved chert beds at the tops of turbidite deposits. We first report field and petrological criteria that allow us to infer the origin of the chert and to test both hypotheses of formation. We then use a geochemical approach to investigate the paleo-environment of chert deposition. Our results (1) offer new criteria for chert characterization, (2) provide a better understanding of the role of clastic sedimentation in silica precipitation, and (3) place constraints and open new possibilities on the use of cherts as paleo-environment proxies.

2. Nomenclature used for cherts

In addition to the long-standing debate on chert formation process, the absence of a clear distinction between different chert types hinders our understanding of their formation and their use as proxies of conditions at the Archean seafloor. The most commonly used nomenclatures are based on (1) chert color (e.g. light to dark gray, greenish gray to green, bluish to dark blue, etc.), (2) structure and outcrop organization (e.g. laminated, massive, vein, banded, etc.), and/or (3) minor components (e.g. carbonaceous, ferruginous, argillaceous, tuffaceous, etc.). Such terminologies, although useful for descriptive purposes, provide little information on the origin of chert, and they vary widely from one author to another.

Van den Boorn et al. (2007) were the first to propose a nomenclature based on the formation process and we adapt their scheme in this paper. (1) Primary cherts are defined as primary chemical precipitates. We conserve the term “C-chert” (i.e. chemical-chert) of Van den Boorn et al. (2007) for oceanic precipitates (Fig. 1a) on the ocean floor and for primary, early diagenetic cement in the uppermost sedimentary layers. (2) We introduce the term “F-chert” (i.e. fracture-filling chert) for discordant and concordant chert precipitated in veins/fractures (Fig. 1b) from fluids that circulated through the crust (e.g. hydrothermal fluids, diagenetic fluid escapement, shallow seawater circulation). (3) Secondary cherts, or “S-cherts”, differ from the other cherts in that they result from the replacement by Si-metasomatism of a sedimentary or volcanic protolith (Fig. 1c), either during percolation of low-temperature seawater or by circulation of low- to high-temperature silica-rich hydrothermal or diagenetic fluids. This nomenclature is illustrated in Fig. 1. As with most geological classifications, the differences between the three types of chert are not always well defined but the classification is useful to distinguish rocks forming by the three main chert-forming processes.

3. Geological background and scientific approach

Archean rocks of the Barberton Greenstone Belt (3.57–3.21 Ga), in South Africa and Swaziland, include a well-preserved volcano-sedimentary succession known as the Swaziland Supergroup (e.g. Viljoen and Viljoen, 1969b; Lowe and Byerly, 1999). The Sandspruit and Theespruit Formations are the oldest and most highly metamorphosed parts of the belt. They mark the base of the sequence and are overlain by three thicker and more extensive units: the mafic- to ultramafic-volcanic dominated Onverwacht Group (3570–3334 Ma), further divided into the Komati, Hoogge-noeg, Kromberg and Mendon Formations, the argillaceous Fig Tree Group (~3258–~3226 Ma), and the arenaceous Moodies Group (~3223–3240 Ma) (see the following papers for further stratigraphic details: Viljoen and Viljoen, 1969a; Armstrong et al., 1990; Kröner et al., 1991; Heubeck and Lowe, 1994; Kamo and Davis, 1994; Lowe and Byerly, 1999; Tice and Lowe, 2004; Hofmann, 2005; Brandl et al., 2006; de Wit et al., 2011; Furnes et al., 2011; Heubeck et al., 2013).

The studied site is located on the eastern limb of the Onverwacht anticline (Fig. 2a). Cherts and silicified sedimentary and volcanic strata are common in this well-exposed type section along the Komati River. They form part of the Kromberg Formation, in a unit referred to as the Noisy Formation by Biggin et al. (2011). Along the banks of the river, within the Songimvelo Nature Reserve, a 200 m-thick sequence of well-bedded clastic sedimentary rocks outcrops continuously and consists mainly of upward-fining conglomerates, diamictites and turbiditic sandstones (Fig. 2b). This section has been widely studied to constrain the depositional setting of some of the world’s oldest siliciclastic deposits and to better understand regional tectonic processes (e.g. Viljoen and Viljoen, 1969a; Lowe

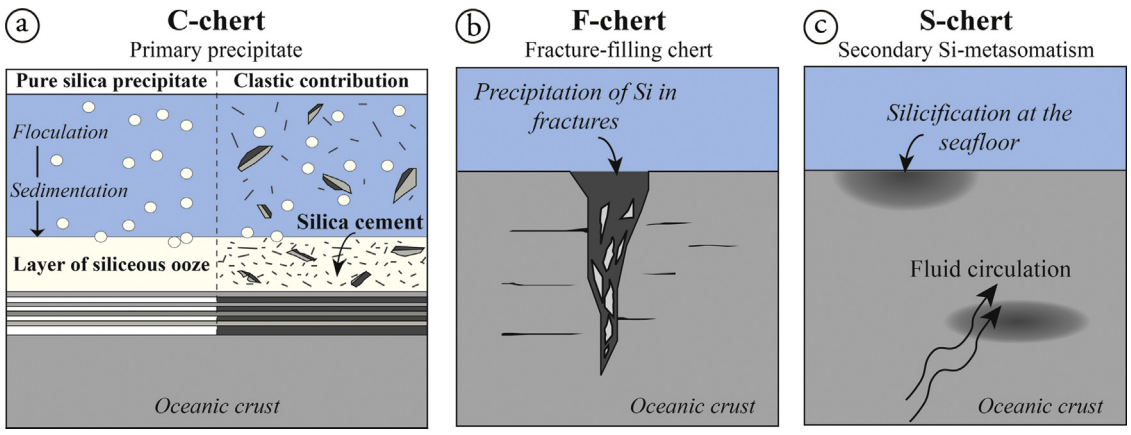

Fig. 1. Nomenclature based on chert formation processes. (a) C-cherts formed from the precipitation of marine silica at the seafloor, either as pure siliceous ooze or as cement between clastic components. (b) F-cherts are chemical precipitates formed in veins or fractures from circulating fluids within the oceanic crust (e.g. low to high temperature hydrothermal fluids). (c) S-cherts are the replacement products of any sedimentary or magmatic protolith subjected to Si-rich fluid circulation (e.g. oceanic, hydrothermal, diagenetic, or metamorphic fluids).

and Knauth, 1977; de Wit et al., 1987a,b, 2011; Armstrong et al., 1990; Lowe and Byerly, 1999; Grosch et al., 2011).

The stratigraphically uppermost units consist of normally graded to massive beds of fine- to coarse-grained volcaniclastic sandstones (up to 5 m thick) (Grosch et al., 2011). Some of these show features commonly found in modern Bouma sequences deposited from low-density currents, such as graded bedding, cross-bedding near the top and flame structures at the contact with the overlying clastic deposit (Fig. 2c). On the basis of lithologies and their sedimentary structures, Lowe and Knauth (1977) interpreted these rocks as tuffs and felsic volcanics reworked as turbidites in a shallow marine environment. Grosch et al. (2011) prefer a shallow, intra-continental epeiric sea setting and proposed that the unit was emplaced "during tectonic uplift of an [. . .] oceanic basin, with turbidite deposition occurring during or after orogenic activity at 3.432 Ga". The cherts in this stratigraphic section occur as thin beds in the uppermost parts of several turbidite beds (Figs. 2c and 3a).

We focused our research on these cherts, with the specific aim of determining whether they are (1) the product of contemporaneous clastic sedimentation and precipitation of marine silica (C-chert) or (2) the result of subseafloor silicification of volcaniclastic deposits (S-chert). In the first hypothesis, the chert would represent the terminal members of Archean Bouma sequences (i.e. Te division) and all the phases within it have been deposited from seawater: components such as feldspar, phyllosilicate and associated phases are interpreted as detrital whereas the siliceous fraction is presumed to result from the diagenic evolution of a chemical precipitate of amorphous silica. Because the terminal members of similar turbidite deposits in modern settings consist of very fine shale and/or mud, Lowe and Knauth (1977), Lowe (1999) and Rouchon et al. (2009) preferred the second hypothesis. According to these authors, the fine-grained clay minerals were replaced during diagenesis by secondary silicates while preserving the morphology and partially the mineralogy of the larger clastic grains. They propose pervasive seawater infiltration, diagenetic fluid migration and/or

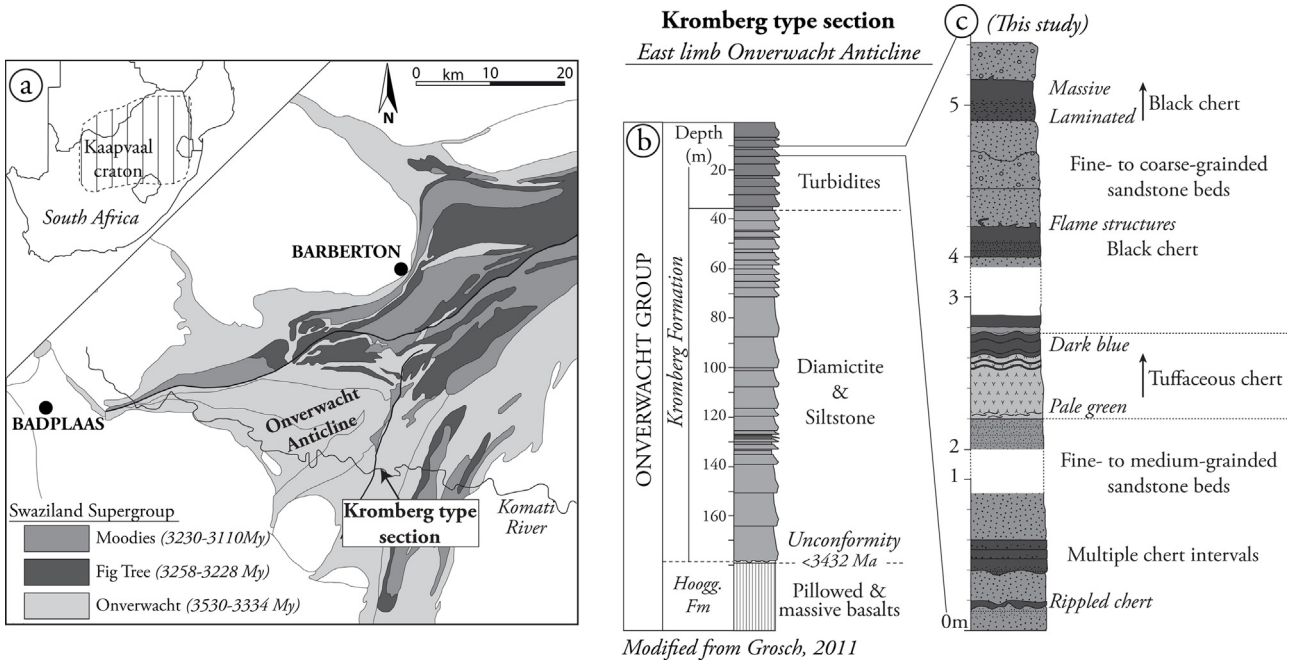

Fig. 2. (a) Simplified geological map of the Barberton Greenstone Belt with the Komati River site location on eastern limb of the Onverwacht anticline. (b) Simplified stratigraphy of the Kromberg type section showing the evolution from basaltic units through to clastic deposits. This study focuses on the uppermost turbidite layers. (c) Cherts in the uppermost part of turbidite beds.

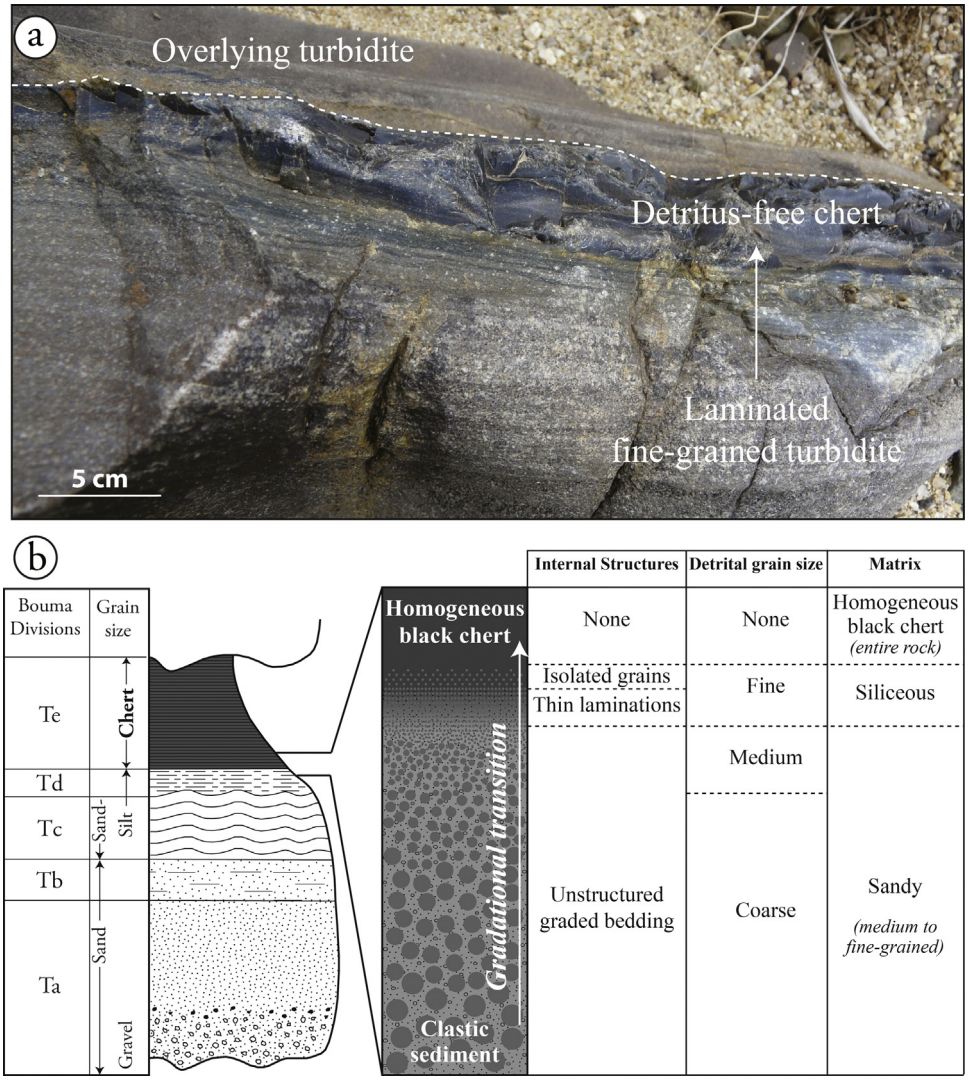

Fig. 3. (a) Field photo of the uppermost layers of Kromberg Bouma sequences showing the evolution from laminated siltstone to homogeneous chert. (b) Schematic description of the siltstone-to-chert transition showing the gradational changes in the abundance and size of detrital grains and in the matrix composition.

hydrothermal fluid circulation to account for the silicification process. In the C-chert hypothesis, the silica in the chert precipitated directly from seawater.

The rocks of the Kromberg type section were metamorphosed under greenschist facies conditions (215 to <350 °C; Grosch et al., 2012), a process that changed clay minerals to sericite and amorphous silica to microcrystalline quartz. In the following descriptions the metamorphic mineral names will be used, with reference when necessary to the original phases. Because of this metamorphism, primary textures in the silica are lost and little information remains about its origin. Additionally, primarily deposited detrital grains may not have been pristine at the time of turbidite emplacement: they could have been altered during weathering and erosion, and could perhaps have been derived from precursors that themselves could have been metasomatised (i.e. silicification with potassium addition). Thus, to distinguish between the two hypotheses of chert formation, clues can be obtained by considering in detail the nature, origin and alteration history of various mineral phases associated with the silica. The approach we adopted is to identify features consistent with primary precipitation, on one hand, and of replacement, on the other.

Mineral assemblages of modern and ancient igneous and sedimentary rocks affected by Si- and/or K-metasomatism are well documented (e.g. Alt and Teagle, 2003; Behnia et al., 2003, 2004; Hofmann and Harris, 2008). Under pervasive Si-rich fluid circulation, the rock progressively alters to a more potassic and siliceous composition by the replacement of primary volcanic material such as feldspar (plagioclase, sanidine, albite), ferro-magnesian silicates (e.g., pyroxene, biotite) and volcanic glass, by a secondary assemblage of K-feldspar, clay and microquartz (e.g. Chapin and Lindley, 1985). Metasomatic minerals first appear as inclusions within larger precursors, then grow to form larger islands before the primary mineral is almost completely replaced, leaving only small remnants within the new crystals (Behnia et al., 2004). Primary sedimentary structures and precursor mineral textures may be well preserved (Schopf and Packer, 1987; Walsh, 1992; Altermann and Kazmierczak, 2003; Orberger et al., 2006; Westall et al., 2001).

Accordingly, if Kromberg cherts resulted from silicification and K-metasomatism after deposition of mudstone at the top of the Bouma sequence, then (1) the clastic grains should show signs of Si- and K-metasomatism (e.g. crystal overgrowths, zonation, replacement features) and (2) such processes would tend to homogenize the feldspar grain composition toward a more potassic endmember. In contrast, if the chert consists of marine silica deposited together with clastic particles, then the detrital content should be as heterogeneous as it(s) source(s). Thus, even if the grains were derived from previously metasomatised rocks, they may show a range of morphologies, mineralogy as well as degree of

alteration. Hence, to obtain criteria for chert identification, we focus on the field relationships, petrographic and mineral compositions of cherts and siltstones from the Kromberg type section exposed along the Komati River.

4. Samples and methods

Samples for petrological and geochemical study were taken from the uppermost 20 cm of turbiditic units, covering the transition from siltstone through to the cherty strata. A range of techniques was used for the petrographic characterization of cherts and siltstones, with the final aim to obtain a maximum of criteria to distinguish the origin of the clastic particles:

- Inspection of thin sections provides essential information about the nature and characteristics of the detrital phases (size, form, degree of alteration, etc.) and their relationship to the microquartz in both the siltstone and the chert.
- X-ray microfluorescence allows the scanning of broad areas and produces chemical maps across the siltstone-to-chert transition. Chemical data are converted to mineral maps using the Supermaps software developed by Ulrich (2010), highlighting the distribution of microquartz, phyllosilicates and feldspars.
- Microprobe chemical maps and associated BSE (*back-scattered electron*) imaging are used to determine the nature of clastic grains as well as features inherited from alteration (e.g. metasomatism, metamorphism).
- Cathodoluminescence is used to determine the metasomatized or magmatic nature of feldspars and to investigate possible chemical changes within the microquartzitic matrix across the siltstone-to-chert transition.

Additionally, major and trace element data were obtained by ICP-AES and ICP-MS following a procedure adapted from that of Chauvel et al. (2011). A detailed description of all the above techniques (i.e. procedures, parameters, accuracy) is given in Inline Supplementary Material.

5. Field description

Although the turbidites are not the primary objective of this study, we describe them in some detail because they help define the sedimentary context in which the cherts were deposited. The turbidites form thick, 1–5 m beds with internal organization typical of a Bouma sequence (Bouma, 1962). They are well sorted, with systematic upward grading from coarse- to medium-grained conglomerate and sandstone (1–3 mm) at the base to fine-grained and commonly laminated siltstone and mudstone (<1 mm) at the top (Fig. 3). The laminated fine-grained upper parts of these turbidites evolve to massive and homogeneous black chert forming either single beds (2–25 cm thick) (Fig. 3a) or several layers that can reach up to 20–30 cm in total thickness. Subangular to rounded clasts of dark chert (2–8 cm in size) may be found either in the first 10 cm overlying the erosional bases of turbidites or forming individual horizons within massive sandstone beds (Fig. 4a).

The upper limit of each chert beds is in sharp contact with the overlying clastic deposit, whereas the lower limit grades from the underlying coarse- to medium-grained lower facies of the turbidite. From bottom to top, over an interval of 2–3 cm (as shown in Fig. 3c), we first observe a decrease in the abundance and size of clastic grains, from silt- to clay-sized, and the appearance of thin laminations that give way to rippled or cross-bedded structures presumably produced by current action (Fig. 4b). Over the same interval, the matrix changes from fine clay to microcrystalline quartz, and, with the disappearance of the uppermost clastic grains and laminations, the rock evolves to homogeneous translucent black chert (Fig. 3). The upper limit of the chert beds is marked by an abrupt reappearance of clastic particles. The contact is sharp and commonly deformed to produce well-developed flame structures (Fig. 4c).

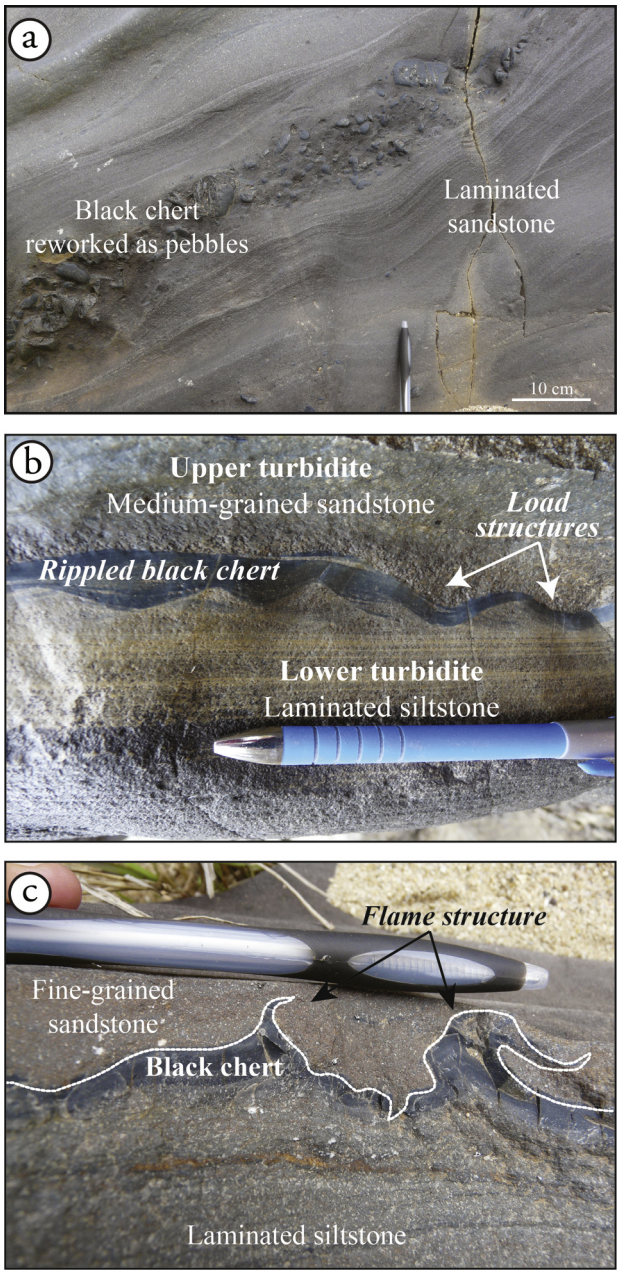

Fig. 4. Deformation structures in Kromberg cherts: (a) chert pebbles in a single horizon between sandstone units; (b) evolution from laminated to rippled siltstone, then to rippled chert at the top of turbidite deposit; (c) load-induced flame structures developed in a chert horizon at the contact with overlying sandstone.

6. Petrography

6.1. Siltstone

The siltstones are composed of clastic grains cemented by microquartz (Fig. 5a), itself containing variable white mica content (up to 30%). The clastic grains are highly variable in shape, size, mineralogical characteristics and degree of alteration (Fig. 5).

Most of the clastic fraction comprises very fine sand- to silt-sized feldspars (200–800 μm) and phyllosilicates (10–50 μm) in roughly

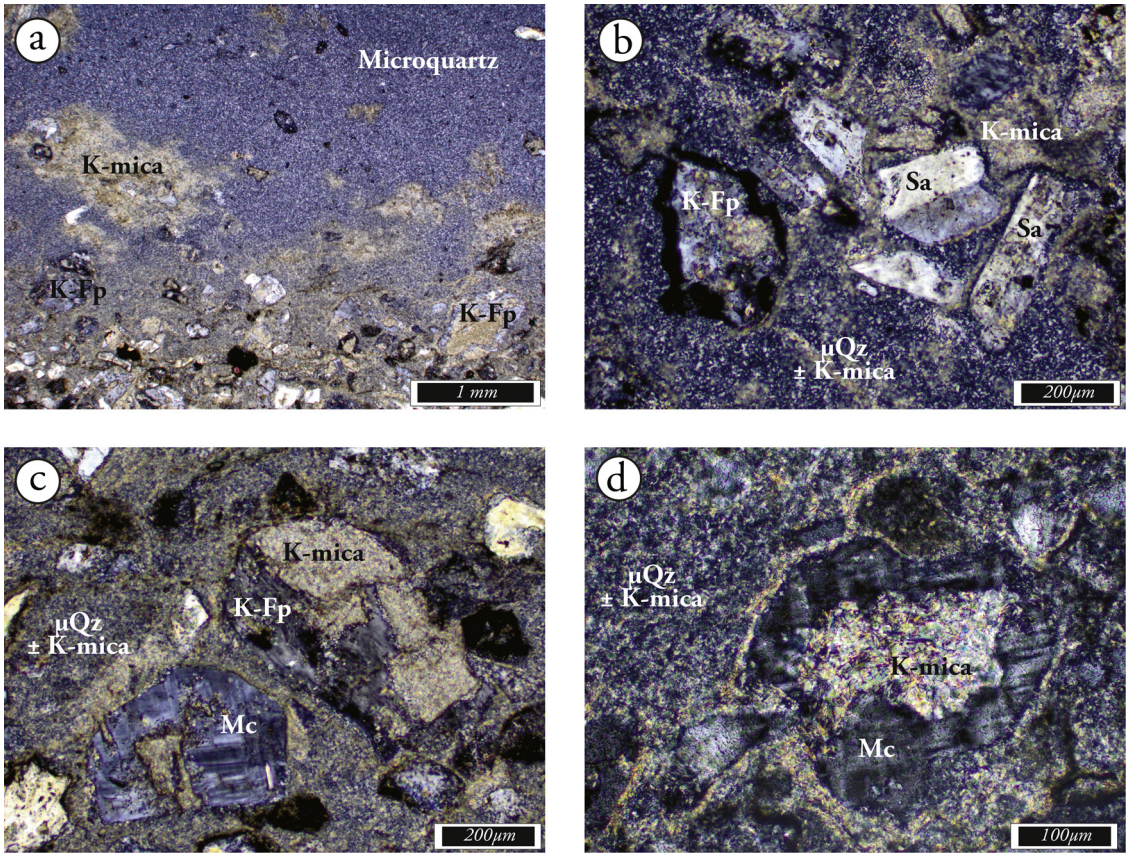

Fig. 5. Photomicrographs of siltstone facies (plane polarized light). (a) Siltstones consist of a heterogeneous detrital fraction enclosed in a matrix of microquartz containing up to 30% phyllosilicates. The evolution to chert (top of photo) is gradational and characterized by a decrease of micaceous and clastic content and increase of the siliceous fraction. (b) Well-preserved K-feldspars with Carlsbad twins typical of sanidine precursors. (c) K-feldspar variably altered to sericite. (d) Microcline grains are sub-rounded and preserve twins that are cut at grain edges. Some feldspar grains are coated by K-mica rims µQ = microquartz; K-Fp = potassium feldspar; Sa = sanidine; Mc = microcline.

equal proportions (Fig. 5). Also present in this assemblage are: (1) a limited fraction of heavy minerals including Ti-oxide, pyrite, zircon and epidote (<2% and less than 50 µm), (2) ovoid agglomerates (lithic fragments) of mud-like material (100–800 µm; Fig. 6c and d), (3) rounded grains (100–200 µm) entirely composed of mesoquartz (Fig. 6c), and (4) abundant grains of feldspar or lithic material (50–400 µm) surrounded by thin rims or coats of Ti-oxides and a brownish-black material that resembles carbonaceous matter (Figs. 5b, 6a and b). These dark rims enclose variable mosaics of microquartz and sericite with more or less preserved feldspar fragments, some of which having twins and elongated shapes typical of sanidine (Fig. 6a and b). We note the near absence of large quartz grains (>200 µm) in the clastic fraction, in agreement with the descriptions of Rouchon et al. (2009) who reported low amounts of such grains even in the deepest and coarsest part of turbidite layers (i.e. in coarser sandstone with lithic fragments). Detrital quartz is present, however, as small (<200 µm), angular fragments disseminated through the siltstone. Very few carbonate grains (<1%) are observed in the siltstone. Their rhombohedric shapes, lack of zoning and tendancy to overprint the microquartz cement suggest they formed as secondary phases during diagenesis and associated carbonatation processes (Rouchon et al., 2009).

Electron microprobe analyses of clastic grains in the siltstone are given in Table 1 (complete data set available in Inline

Table 1
Microprobe analyses of (i) an internal standard of orthoclase, (ii) micro-feldspars and microquartz in cherts, (iii) K-feldspars and sericite in siltstones. n = number of data. 1σ = standard deviation from average concentrations. The deviation is low compared to the number of data, showing the homogeneity in the chemical composition of clastic grains. K-feldspars have low sodium content compared to standard values, which is typical of minerals formed during metasomatism.

	Standard – orthoclase		Kromberg River							
			Black chert				Laminated siltstone			
			K-Feldspath		Quartz		K-Feldspath		Sericite	
(wt%)	n = 12	1σ	n = 6	1σ	n = 2	1σ	n = 32	1σ	n = 6	1σ
SiO_2	65.0	0.21	65.2	0.68	98.7	0.50	65.1	0.51	48.7	0.52
TiO_2	<0.01		<0.01		<0.01		<0.01		0.54	0.04
Al_2O_3	18.5	0.07	18.0	0.28	0.33	0.27	18.2	0.37	34.5	0.48
FeO	0.03	0.02	0.03	0.02	0.03	0.01	0.02	0.02	0.85	0.03
MnO	0.01	0.01	0.01	0.01	0.00	0.00	<0.01		<0.01	
MgO	<0.02		0.01	0.01	0.01	0.01	<0.02		1.66	0.08
CaO	<0.01		<0.01		<0.01		<0.01		0.01	0.01
Na_2O	1.40	0.02	0.17	0.02	0.02	0.01	0.17	0.02	0.10	0.02
K_2O	14.9	0.06	15.8	0.44	0.10	0.07	15.9	0.48	8.22	0.29
Total	100.0		99.3		99.2		99.4		94.6	

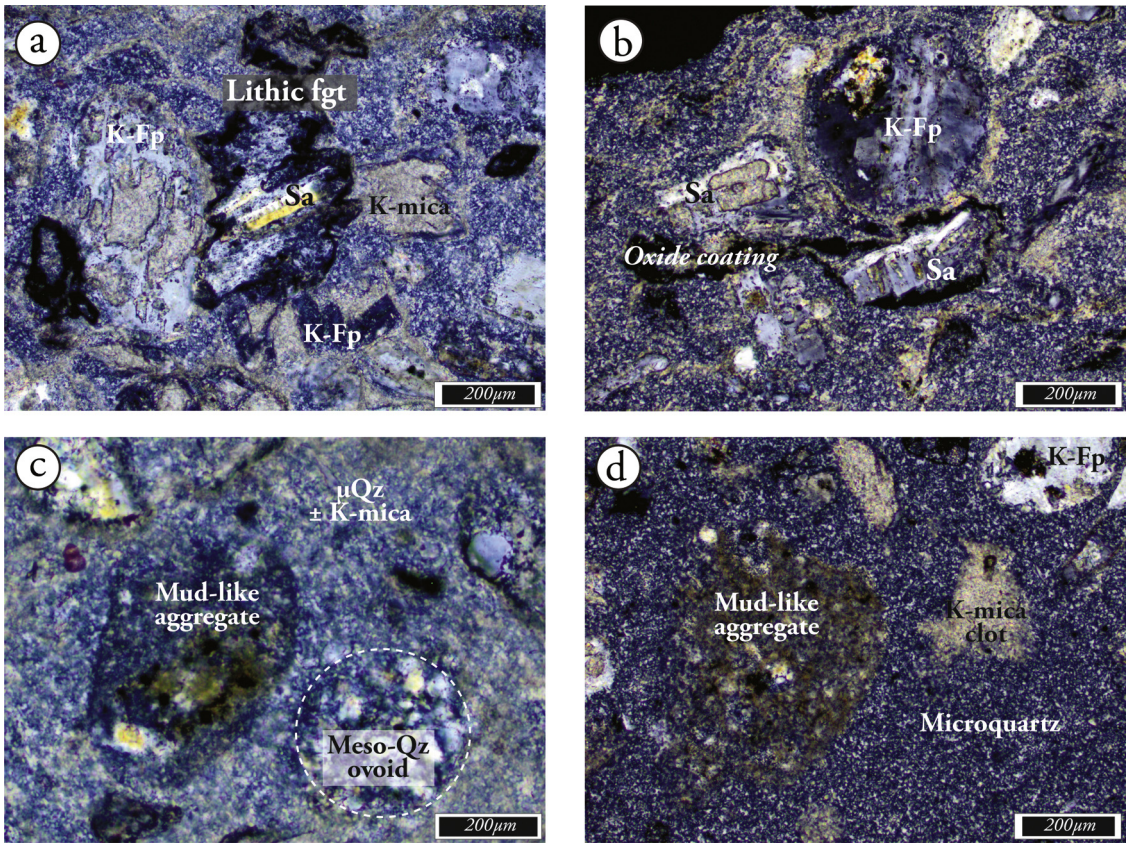

Fig. 6. Clastic grains in cherts, including: lithic fragments coated by oxides and carbonaceous matter and enclosing sanidine grains (a, b), rounded to angular grains of K-feldspar preserving Carlsbad and microcline twinning (b), mud-like aggregates (c, d) and mesoquartz ovoids (c). All these are enclosed within a siliceous matrix in which phyllosilicates may be abundant and/or concentrated in small clots (d). µQ = microquartz; K-Fp = potassium feldspar; Sa = sanidine; Mc = microcline; Lithic fgt = lithic fragment.

Supplementary Table S2). The compositions of all the analyzed feldspars ($n = 32$) are close to a pure, potassic endmember and contain less than 0.2 wt% of Na_2O. The phyllosilicates are K-micas of sericite or muscovite composition (Table 1). They are similarly depleted in sodium ($Na_2O = 0.1$ wt%), but are enriched in magnesium (MgO = 1.66 wt%). Both mineral types are unsilicified, as shown by stoichiomeric SiO_2 contents of 65.2 wt% and 48.7 wt%, respectively.

Inline Supplementary Table S2 can be found online at http://dx.doi.org/10.1016/j.precamres.2014.10.009.

The feldspar grains display a wide range of characteristics. Some are partially replaced by fine-grained clay minerals, but the least altered grains preserved primary textures, shape and twinning typical of orthoclase, microcline, and sanidine, as shown in Fig. 5b and c. These grains are the coarsest, reaching up to 800 µm in size, and have angular shapes for sanidine (Figs. 5b, 6a and b) to rounded shapes for microcline grains (Fig. 5d). They have uniform internal compositions (i.e. no zonation), and sharp to crenulated boundaries (e.g. Fig. 5c) often delineated by sericite rims (Figs. 5d and 6b). As shown in BSE image and microprobe maps of Fig. 7, the small crenulations (<1–2 µm) have restricted extent and represent microembayments of silica. On the other hand, feldspar cores are largely replaced by phyllosilicates (<20 µm in size) along cleavage traces (Figs. 5–7). This alteration affected most of the clastic fraction but to a variable extent (e.g. Fig. 5b and c). The smallest feldspar grains (<200 µm) usually are completely replaced such that only ghosts composed of clouds of micaceous minerals remain. A third type of texture involves the homogeneous disturbance of primary twinning of some feldspars, leading to a microcline- or perthite-like texture as shown in Fig. 5c. This particular texture contrasts with other microcline grains that show rounded shapes, and twins that are cut at the grain boundaries, an example of which is presented in Fig. 6c and d. Finally, in the cathodoluminescence map of Fig. 8, the uncoated feldspar grains have a dull, yellowish luminescence that contrasts with the bright blue color of the grains coated by carbonaceous matter and oxide material (black arrows in Fig. 8).

The cement between clastic grains is largely composed of microquartz in association with large proportions of fine-grained phyllosilicates (up to 30%; Figs. 5 and 6). Microquartz grain boundaries are well defined, the grain size is homogeneous through the matrix (<5–10 µm) and traces of chalcedony precursor are rare. Phyllosilicates in the matrix are sericite similar to those found in feldspar embayments in terms of optical and chemical properties (Table 1). They are irregularly distributed, commonly but not systematically located near feldspar boundaries (e.g. Fig. 5d and 6b). Entirely coated grains such that in Fig. 5d are rare. Instead, sericite grains form concentrated zones in the matrix, either by alignment along structures that resemble fluid circulation pathways (e.g. Fig. 6b), or by agglomeration in small clots (e.g. Fig. 6d).

6.2. Transition from siltstone to chert

The topmost part of turbidite layers – the gradational evolution from siltstone to chert – is first marked by the disappearance of detrital grains, laminations and other sedimentary structures as shown in Fig. 5a. In the microphotographs and cathodoluminescence map of Fig. 8, isolated feldspar grains float in a microquartz matrix above the siltstone-to-chert transition. Some of these grains are large (>500 µm), almost completely fragmented and altered to phyllosilicates; others are smaller (>200 µm) with well-preserved twinning, angular shapes, and no significant alteration. These grains

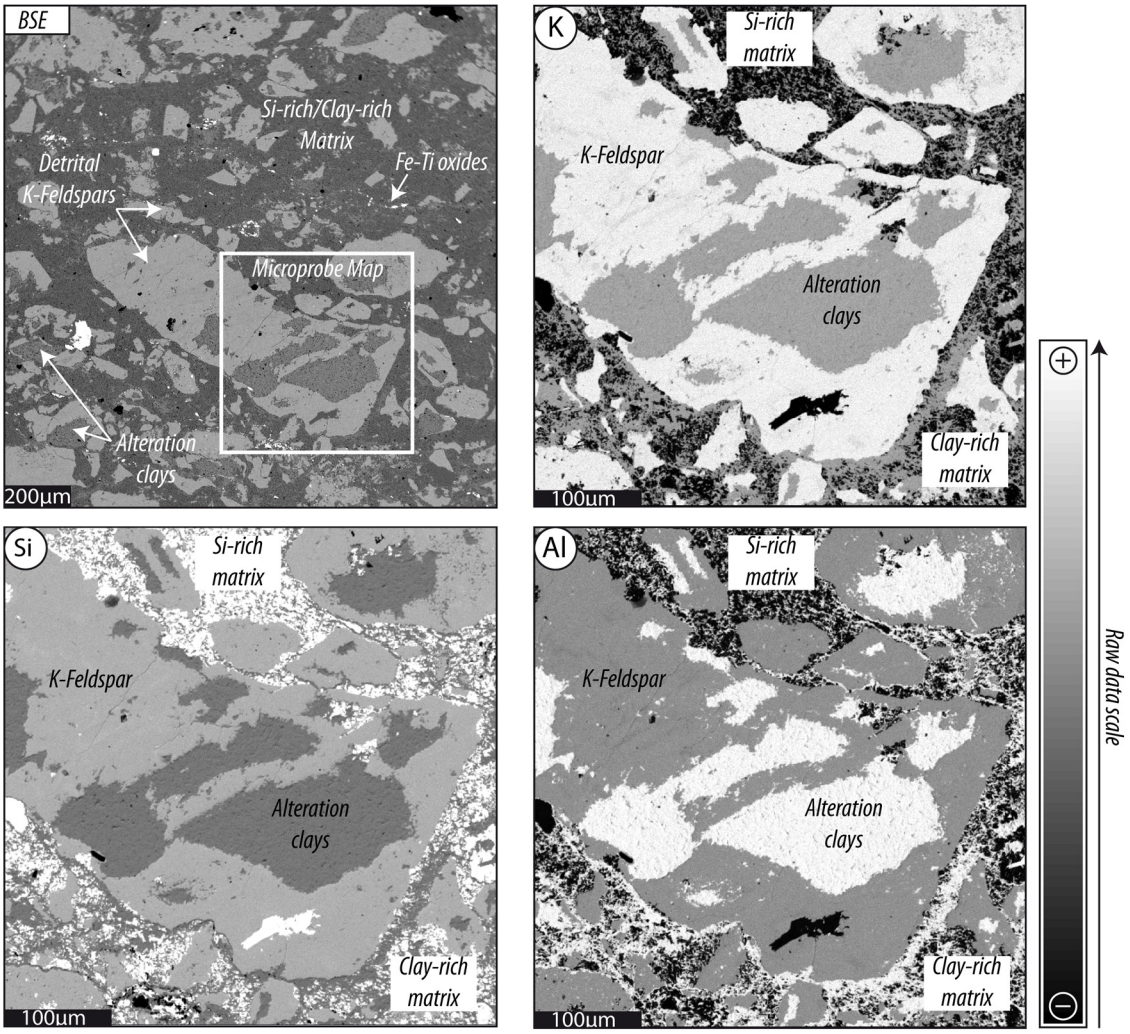

Fig. 7. Back-scattered electron (BSE) image (upper left) and microprobe chemical maps (K, Al and Si) of siltstone. Potassium feldspars have sharp boundaries partially crenulated by silica micro-embayments. Alteration to phyllosilicate is common along cleavages. The surrounding matrix is essentially siliceous and contains abundant phyllosilicates, either homogeneously distributed or concentrated at feldspar boundaries.

are chemically indistinguishable from feldspars in the underlying siltstone as shown by their similar, yellowish luminescence.

In the same interval, the microquartz matrix appears to be in continuity from the siltstone through the chert, evolving gradually in its phyllosilicate-to-silica ratio. This is particularly evident in Fig. 9. In the siltstone, detrital feldspars are readily visible and surrounded by microquartz mixed with about 30% of phyllosilicates. Less than 1 mm higher, the sericite content is abruptly diluted to less than 15% whereas the silica fraction increases to more than 85%. Such a continuous evolution strongly resembles a classic graded sedimentary sequence: over a mere centimeter, the sediment evolves from clastic to chemical with decreasing particle and increasing siliceous contents.

Inline Supplementary Fig. S1 can be found online at http://dx.doi.org/10.1016/j.precamres.2014.10.009.

6.3. Chert

Above the gradational contact, after the disappearance of most clastic grains and internal laminations, the chert seems homogeneous (Fig. 5a and 10a). Nonetheless, it contains a significant proportion of fine-grained particles that can be identified by X-ray diffraction (Fig. 11) and microprobe analyses (Table 1). The chert consists of a mixture of homogenous microcrystalline quartz (5 μm mean crystal size), sericite (<10 μm) and minor isolated, very fine-grained K-feldspar (<60 μm) (Figs. 10 and 11). Together, K-mica and K-feldspar represent less than 15% of the thin section area. Whereas the majority of K-micas are homogeneously distributed, rare and isolated micaceous clumps (<400 μm in total size) are found enclosed in the silica matrix (Fig. 10b).

As illustrated by the cathodoluminescence (Fig. 8) and microprobe maps (Fig. 12), the feldspar grains have variable shapes from angular to irregular. They are isolated within the microquartzitic matrix and are chemically undistinguishable from the larger feldspar grains in the underlying detritus-rich facies, with average SiO_2 concentrations of 65.2 wt%, 18 wt% Al_2O_3, 15.8 wt% K_2O, and very low Na_2O (0.17 wt%) (Table 1). Minor proportions of very fine-grained sericite-like minerals (5 μm) are disseminated within the microquartzitic fabric (Fig. 12). They are uniformly distributed and not preferentially associated with micro-feldspars. As shown in Fig. 12, micro-sericite occupies interstitial positions in between microquartz grains. Microquartz is the main component of the chert and comprises 80–90% of its volume.

7. Evidence for the primary origin of cherts

The paragenesis of the cherts and siltstones of the Kromberg type section is dominated by K-feldspar, K-mica and

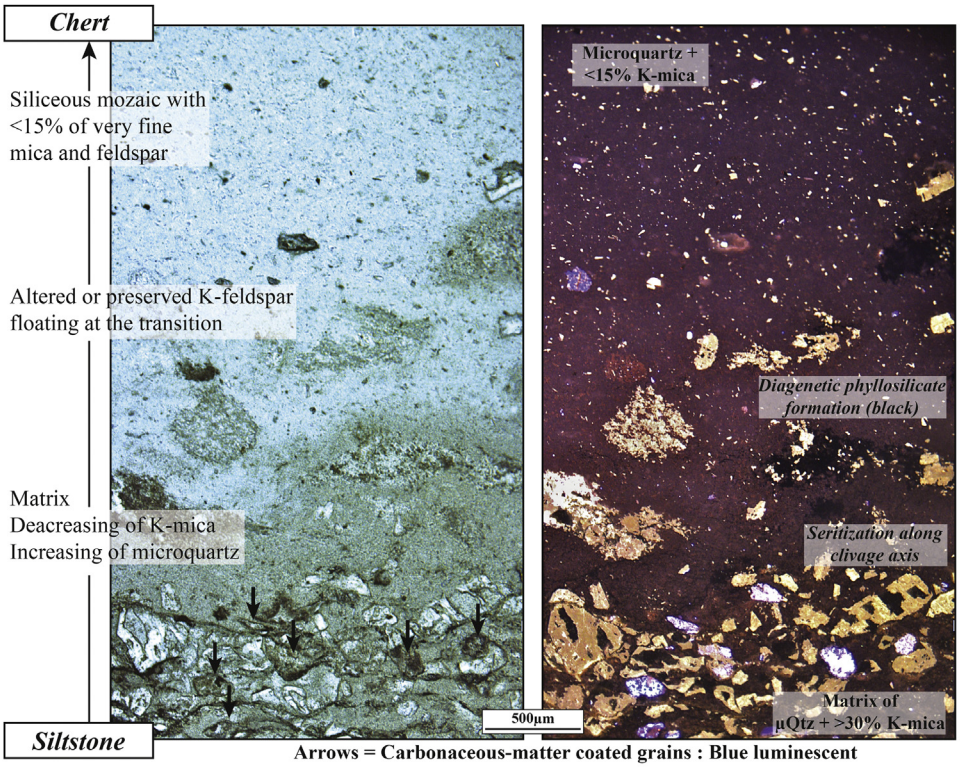

Fig. 8. Optical profiles and cathodoluminescence map at the siltstone to chert transition. Notable features are (i) the presence of altered and well-preserved feldspars isolated in a microquartz matrix above the contact, (ii) the abrupt decrease of mica content in the matrix from 30% in the siltstone to less than 15% in the chert, and (iii) the presence of two families of feldspars, those with yellowish and bluish luminescent grains, the latter being smaller, more rounded and coated by carbonaceous matter.

microquartz, and strongly resembles mineral assemblages in modern and Archean volcaniclastic deposits affected by Si- and/or K-metasomatism (e.g. Alt and Teagle, 2003; Behnia et al., 2003, 2004; Hofmann and Harris, 2008; Rouchon et al., 2009). However, several observations suggest that such metasomatism occurred mainly before turbidite deposition, and that while most of the clastic fraction at Komati River is of detrital origin, most of the silica precipitated from ambient, marine fluids:

7.1. Variability of the composition of clastic particles

One key observation is the presence of orthoclase, microcline and sanidine, as distinguished by optical characteristics such as preserved twins. Such heterogeneity, in addition to the presence of coated grains, detrital mica aggregates, and mud-like lithic fragments, points to diverse sources to the sediment and supports a detrital origin for most of the silicate grains. Moreover, the fact that some microclines are rounded and show twins cut at grain edges (Fig. 6c and d) confirms that part of these issued from the erosion of igneous or metasomatised rock.

7.2. Restricted in situ alteration of detrital grains

The following observations suggest that most alteration occurred prior to erosion and sedimentation whereas post-deposition alteration of K-feldspars was restricted to low temperature, diagenetic conditions:

- The wide range of seritization of feldspars (Figs. 5 and 6) implies that they underwent different conditions during alteration. In this collection of detritus, the least altered grains give a maximum estimate for the alteration degree reached by the whole fraction. As previously described from Fig. 6b, part of K-feldspars is well preserved and lacks significant phyllosilicate replacement.
- The lack of sericite coating around most of K-feldspars, which normally forms during diagenetic metasomatism of volcaniclastics, can be explained by its removal during transport through to deposition site, then by weak in situ seritization.
- Additional evidence that favors limited, in situ metasomatism are the limited extent of silica embayments at feldspar boundaries and the lack of characteristic features such as crystal overgrowths, zonation or protolith remnants in neo-formed crystal lattice (e.g. sanidine or microcline cores surrounded by diagenetic orthoclase or microcline) (e.g. Alt and Teagle, 2003; Behnia et al., 2003, 2004).

7.3. Primary origin of the silica

Through the siltstone-to-chert transition, we see a drastic change in the phyllosilicate content of the siliceous matrix. Over less than 1 cm, it decreases from up to 50% in the siltstone to less than 15% in the overlying chert. If these rocks were formed after the silicification of a silt-like and mud-like precursor respectively, one would expect a stronger effect in the coarser, i.e. more permeable, facies because efficient Si-rich fluid circulations and chemical exchanges would be favored (e.g. Tucker, 1991). We firmly believe that the amount of Si-metasomatism required to transform a mud precursor into a chert comprising more than 85% of microquartz would have resulted in the almost complete replacement of detrital phyllosilicates and feldspars by a mosaic of microquartz + sericite in the siltstone (e.g. Rouchon and Orberger, 2008; Rouchon et al., 2009). Instead, abundant feldspars are well preserved whereas phyllosilicates, both detrital and metasomatic, comprise half of the matrix. Thus, we attribute the disappearance of large clastic grains, contemporaneously with the rapid but gradational increase of the microquartzitic cement through the cherty facies, as a continuous evolution from clastic to chemical sedimentation. Accordingly, we

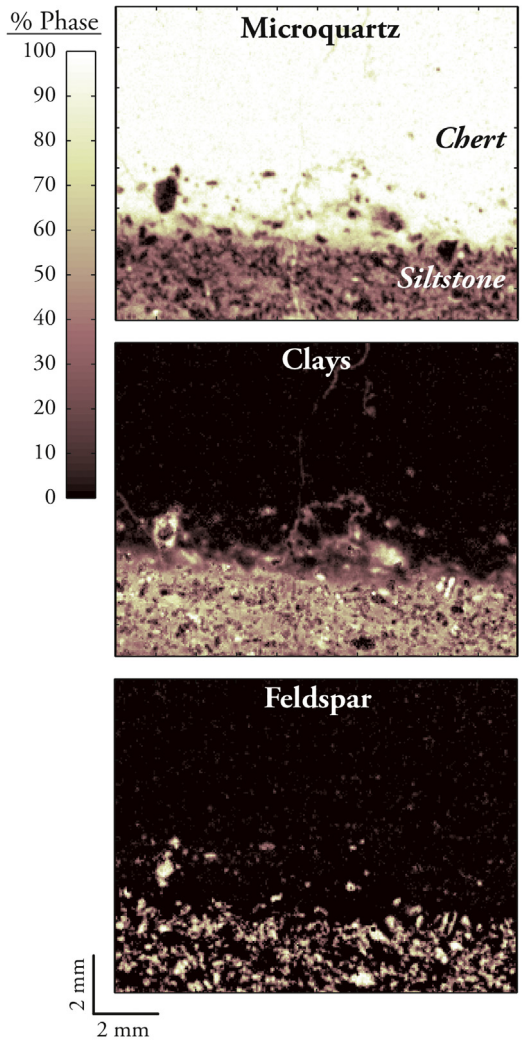

Fig. 9. X-ray microfluoresence maps at the siltstone to chert transition. Chemical images were converted into mineral phase maps using the Supermaps software developed by Ulrich (2010). Inline Supplementary Fig. S1 illustrates the conversion method. Large feldspar grains are abundant in the siltstone and enclosed in a matrix of microquartz mixed with significant amount of sericite. The chert lacks clastic grains and is essentially composed of microquartz. The transition is sharp and characterized by an abrupt decrease in sericite content in the matrix and by the disappearance of clastic grains.

consider that most of the silica is of primary origin and formed part of the depositional event in the sedimentary sequence.

Even though the above arguments point to a detrital origin of the particles, we also found evidence that suggests that many of the K-feldspar grains were metasomatized: (1) their very low sodium contents (0.17 wt%; Table 1), (2) their homogeneous composition close to the pure potassic endmember, and (3) their weak luminescence compared to other grains in Fig. 8 (Kastner, 1971). To reconcile both observations, i.e. that the clastic components include both detrital and metasomatized grains, we argue that a large proportion of them had already been metasomatized prior to erosion. Following deposition, they were further altered to phyllosilicates during burial and diagenesis.

Accordingly, three types of white mica are present in the clastic fraction: the oldest generation is detrital and inherited from the metasomatic alteration of magmatic silicates prior to erosion; a second generation formed by fluid–rock interaction during transport, deposition and early diagenesis and involves the local dissolution and replacement of detrital feldspars; the youngest generation is also diagenetic and formed by the precipitation of authigenic phyllosilicates in pores and diagenetic fluid pathways. All these minerals were probably originally clay (e.g. illite or montmorillonite) now altered to fine-grained muscovite under the low-grade metamorphic conditions that affected this region (215 to <350 °C; Grosch et al., 2012).

In a following section, we discuss a model whereby the Kromberg siltstones and other clastic rocks were deposited from turbidity currents while the silica precipitated from seawater.

8. Geochemical signal in Kromberg cherts

8.1. Major and trace element composition

As shown in Table 2 and Fig. 13, the siltstones in Kromberg Fm. turbidites are rich in Al_2O_3 (6.5–17.9 wt%), $Fe_2O_{3(tot)}$ (0.36–0.39 wt%), K_2O (2.7–7.2 wt%) and TiO_2 (0.17–0.52 wt%), which is consistent with the presence of abundant siliciclastic material in these samples. The overlying cherts also contain significant aluminum (3.3–7.7 wt%) and potassium (1.2–3.6 wt%), which we attribute to the micro-sericite and micro-feldspar recognized in Figs. 11 and 12. The SiO_2 content of cherts (up to 92 wt%) and siltstones (>69.7 wt%) is far higher than those of normal shales (average Archean shales, SiO_2 = 61 wt%, Condie, 1993) due to the abundance of microquartz in both facies.

In Fig. 13b and c, well-defined positive correlation curves (r^2 = 0.92–0.99) are observed between SiO_2 and the continent-derived elements Al, K and Ti, which is consistent with their presence in the clastic fraction. The linear trends are best defined by the siltstones whereas the cherts plot close to each other near the quartz end-member. The consistency across the series suggests that the bulk composition of detrital particles does not vary significantly from one turbidite layer to another. However, it is variably diluted by the microquartzitic content of each sample: in Fig. 13a, the decrease in major element concentrations with increasing SiO_2 is interpreted as an increase in the siliceous over detrital fraction from the siltstone through to the chert.

In Fig. 13b and c, all samples plot on mixing lines between (1) a pure siliceous component (microquartz), and (2) a clastic component dominated by K-feldspar and K-mica. The siliceous component dominates both facies and comprises more than 50% of most siltstones (one sample contains only 35%), and more than 80% of the cherts (Fig. 13b,). Sericite and K-feldspar are present in roughly equal proportions (43% and 57% respectively) and control the entire potassium and aluminum content of the clastic fraction. In the TiO_2 vs. K_2O diagram of Fig. 13c, the correlation curve shows a deviation from the above-modeled composition, which points to the contribution of additional Ti-bearing phases. The Ti/Zr ratio of siltstones ranges from 13.3 to 17.8, which is very close to the average 15.2 ratio of ilmenite and far from the 0.10 value of typical zircons (Garçon et al., 2011). Thus, both the Ti and Zr contents in these samples are probably controlled by Ti-oxides, whose contribution is estimated at 1.2–1.3% from Fig. 13c.

Similarly, the trace element composition of both facies seems largely controlled by the clastic fraction. When taking the aluminum content as representative of the silicate grains, (i.e. K-feldspar and K-mica), positive correlations emerge between the continental-derived elements Zr, Nb, Sc, Ni (and Hf, Ta, not shown) (r^2 = 0.88–0.99) as well as the large ions Cs (r^2 = 0.97) and Rb (r^2 = 0.92; not shown) (Fig. 14b). On the other hand, all these elements are negatively correlated with SiO_2 (r^2 = 0.75–0.97) (Fig. 14a). Thus, most of the trace element characteristics of siltstones and cherts are derived from the detrital feldspars and phyllosilicates, with a signal diluted by the siliceous content. The lack of correlations of mobile elements such as U and Pb as well as Ba and Li (not shown), can be explained by their disturbance during secondary processes that operated during erosion, sedimentation

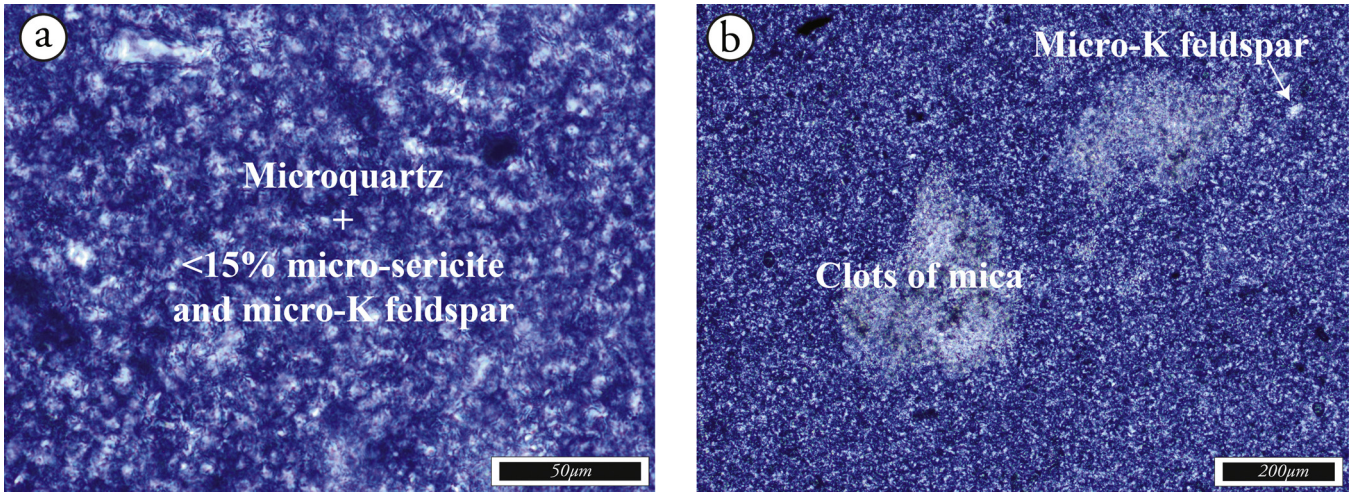

Fig. 10. Photomicrographs of chert layers at the top of turbidites. (a) The chert is homogeneous and exclusively composed of microquartz mixed with <15% of phyllosilicates. (b) Micaceous clots isolated in the microquartz mosaic.

and subsequent burial and metamorphism. The transition metals Cr and Cu (Fig. 14c), also lacking correlation with aluminum, are more likely associated to non-silicate phases (i.e. oxides and other heavy minerals) and may vary from one turbidite layer to another.

To summarize, the major element composition of Komati River siltstones is consistent with a mixture of (1) a clastic fraction essentially composed of 43% sericite, 57% K-feldspars and ≈1% of ilmenite, and (2) a siliceous fraction that varies from about 35% in siltstones to 80–92% in the overlying cherts. Because the siliceous fraction is poor in all major and trace elements other than SiO_2, and because the clastic fraction is far richer in these elements, we cannot access the chemical composition of the silica. Thus, the composition of such clastic-rich cherts cannot be used to infer the origin of the silica (e.g. oceanic vs. hydrothermal), but classic sedimentology is still applicable (e.g. provenance studies). Because we restricted this study to the uppermost 10 cm of meter-scale sedimentary units, such compositions are not representative of the average clastic influx that produced the turbidites, but nonetheless approach the composition of the eroded source.

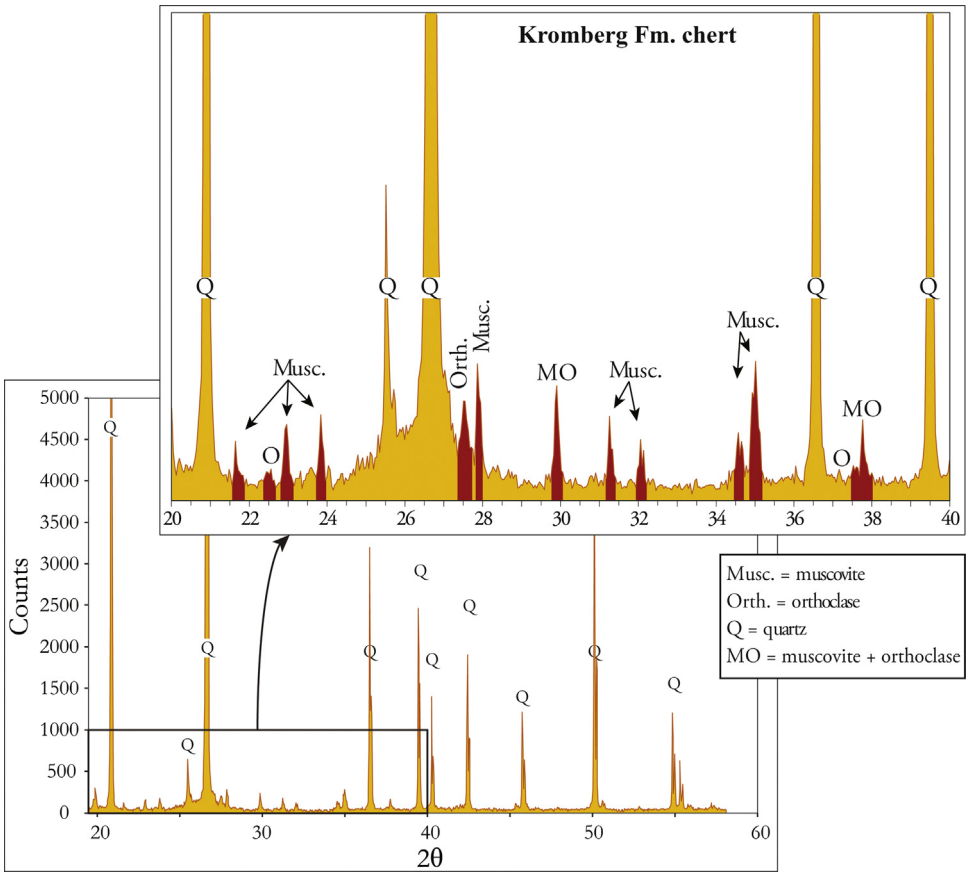

Fig. 11. X-ray diffraction spectra for a chert sample showing an assemblage of microquartz with traces of muscovite (sericite) and K-feldspar (orthoclase). Q = quartz; Musc./M = muscovite; Orth./O = orthose; MO = muscovite + orthose.

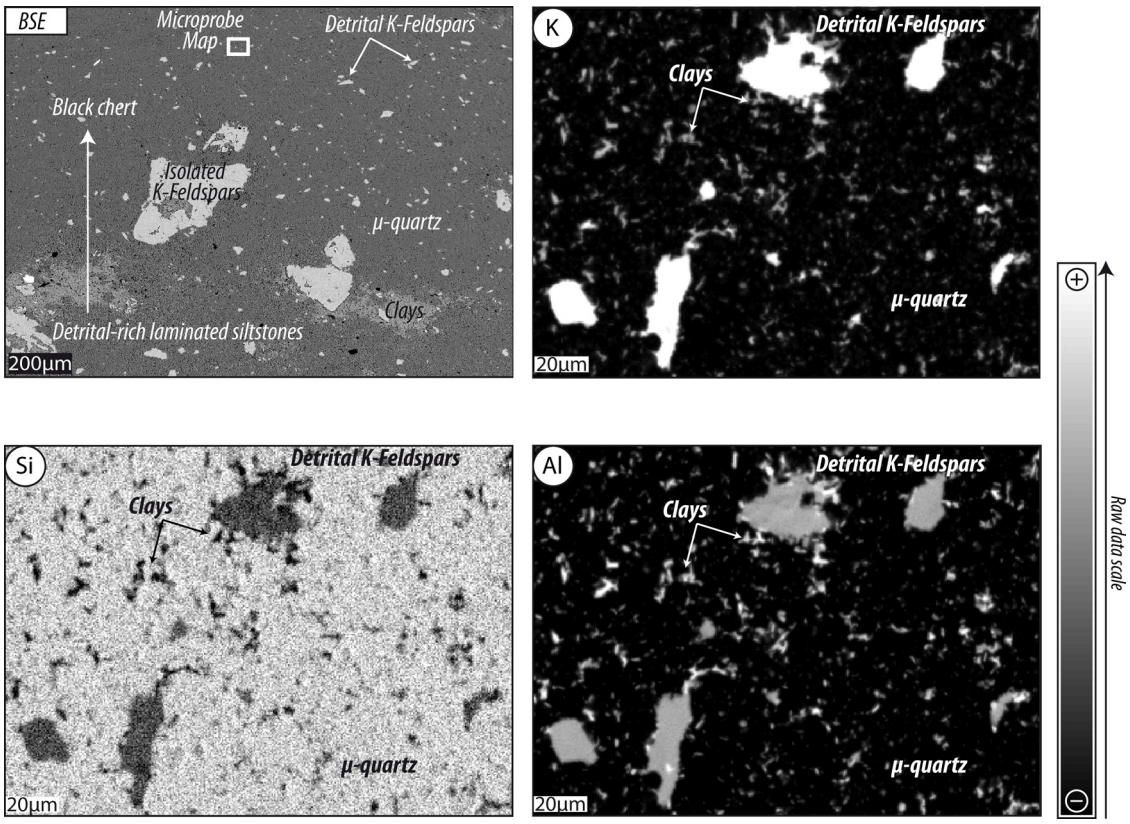

Fig. 12. Microprobe chemical maps (K, Al and Si) in the uppermost chert facies. The chert comprises <15% of sericite and K-feldspar in the form of micrograins and >85% of microquartz. Phyllosilicates occupy interstitial positions within the microquartzitic mosaic.

8.2. REE and origin of clastic particles

Because the REE are supposed to be immobile during secondary processes (e.g. alteration, weathering, diagenesis) (e.g. Bau and Möller, 1993; Bau and Dulski, 1996; Webb and Kamber, 2000; Shields and Stille, 2001; Shields and Webb, 2004; Nothdurft et al., 2004; Bolhar et al., 2004), and because no intense in situ silicification is observed (Section 7), the primitive-mantle normalized REE patterns of Fig. 15 should represent the primary signature of the sediment.

Both cherts and siltstones have strongly fractionated REE patterns (Pr/Yb = 4.0–11.6 and 2.7–10 respectively) consistent with a felsic origin for their clastic content. They are enriched in the light REE whereas the heavy REE are either flat or slightly depleted. Two samples are significantly enriched in cerium with a positive anomaly of 2.3 and 3.4 (calculated as $Ce/Ce^* = Ce_{CN}/(2Pr_{CN}\text{-}Nd_{CN})$ from Bolhar et al., 2004). The Y/Ho ratios are low in average and remain close to or slightly above chondritic values (≈26–28; Pack et al., 2007), ranging from 26.2 to 32.2 in cherts and from 27.1 to 33.4 in siltstones.

Rouchon et al. (2009) advocated a mixed provenance of Kromberg Formation turbidites. These authors proposed that silicified dacites of the Hooggenoeg Formation, previously studied by Hofmann and Harris (2008), were major contributors. These rocks stratigraphically underlie the Kromberg Formation and crop out farther to the north-east. The volcano-sedimentary sequence is dated at the base at 3445 ± 5 Ma (de Wit et al., 1987a) and has been regarded as a dacitic dome and volcanic equivalent to the contemporaneous Theespruit pluton (3445 Ma; de Wit et al., 1987a; Lowe and Byerly, 1999; Rouchon et al., 2009). Silicified dacites are covered by their own erosional products, dated at 3438 ± 12 Ma (Lowe and Byerly, 1999). Below the volcano-clastic transition, dacitic feldspars are altered to sericite and quartz and to an assemblage of K-feldspar, sericite and quartz 100 m deeper in the sequence (Hofmann and Harris, 2008; Rouchon et al., 2009). Rouchon et al. (2009) attribute the K-feldspar, sericite and quartz assemblage to K- and Si-metasomatism and the disappearance of K-feldspars at the top of the unit to evolution to colder and more acid conditions near the contact with Archean seawater.

Both the Hooggeneog dacites and dacitic volcaniclastics (Rouchon et al., 2009), and their assumed plutonic equivalent, the Theespruit pluton, (Abraham, 2010), may contribute to the Kromberg volcaniclastic rocks: both have strongly fractionated, felsic-like REE patterns (Pr/Yb = 9.2–15.4 and 8.8 respectively), with variable depletion in the HREE that cover the range observed in Kromberg cherts and siltstones (Fig. 15). The trace element patterns of Fig. 16 also show additional characteristics shared by the dacites and Kromberg cherts, including a slight enrichment in incompatible elements, a strong depletion in Sr and similar enrichments in Rb, Pb, Zr and Hf. A single dacitic source is however inconsistent with the following observations:

- the concentration of several trace elements in cherts exceeds those measured in the dacites: in particular the trace metals Cr and Co can be 10 times more enriched than the dacites (Fig. 16). Providing these elements are indeed located in detrital phases, such as oxides or other heavy minerals, they indicate the contribution of an additional source to the final sediment.
- although the shapes of dacite spectra are broadly similar to those of the cherts, the REE are less fractionated in cherts and siltstones and show less LREE enrichment and weaker HREE depletion.

The feldspar-rich deeper zone of metasomatized dacites could reasonably have been the source of the metasomatized K-feldspars and associated phyllosilicates of the Kromberg siltstones. The wide variation in the degree of seritization of the feldspars (Figs. 5 and 6)

Table 2
Geochemical composition and selected element ratios for Kromberg cherts and siltstones. <LD = below detection limit. Precision of analyses is given in Inline Supplementary Table S1, which can be found online at http://dx.doi.org/10.1016/j.precamres.2014.10.009.

	Black chert				Laminated siltstone			
	KRC1A-BC	KRC8-BC	KRC11-BC	KRC1B-BC	KRC8-Sed1	KRC8-Sed2	KRC10-Sed	KRC11-Sed
Major elements (wt%)								
SiO_2	89.1	95.1	91.7	85.2	69.7	88.3	81.5	88.8
TiO_2	0.09	0.07	<LD	0.24	0.52	0.17	<LD	0.19
Al_2O_3	4.41	3.33	4.59	7.67	17.85	6.52	<LD	7.34
Fe_2O_3 t	<LD	<LD	0.31	<LD	0.38	<LD	0.39	0.36
MnO	<LD	<LD	<LD	<LD	<LD	<LD	0.01	<LD
MgO	<LD				0.52	<LD	0.25	0.13
CaO	<LD				<LD	<LD	0.65	<LD
Na_2O	0.03			0.04	0.04	0.03	0.03	<LD
K_2O	1.94	1.22	1.73	3.60	7.23	2.71	5.95	3.23
LOI	0.79	0.76	0.66	0.77	2.62	0.78	1.36	0.87
Somme	96.4	100.5	99.0	97.5	98.9	98.5	90.1	101.0
Trace elements (ppm)								
Cs	0.442	0.319	0.386	0.664	1.37	0.547	0.798	0.598
Rb	36.1	33.7	32.5	62.2	163	47.8	79.0	43.0
Ba	40.8	17.9	34.2	61.4	56.6	31.8	47.4	42.6
Th	2.25	2.42	2.55	2.22	2.46	2.34	1.43	1.20
U	0.67	0.375	0.555	0.604	0.577	0.478	0.642	0.551
Nb	2.10	3.07	2.91	3.18	10.3	2.90	6.55	4.00
Ta	0.221	0.265	0.295	0.283	0.667	0.287	0.462	0.338
Pb	5.06	1.16	1.62	1.92	1.03	1.14	1.72	1.69
Sr	2.19	1.18	0.902	2.05	1.74	1.27	1.55	0.861
Zr	48.8	38.1	43.3	88.4	192	63.7	175	82.0
Hf	1.29	0.889	1.31	1.98	4.32	1.6	3.91	2.05
Ti	518	555	531	1354	3424	989	2559	1133
Li	1.69	2.22	1.56	2.67	10.4	3.71	4.36	2.25
Sc	1.4	0.884	0.93	1.83	4.16	1.49	2.95	0.935
V	12.8	11.8	15.9	17.4	36.1	13.3	22.5	17.6
Cr	8.48	12.2	246	21.7	64.9	17.2	189	226
Co	21.2	0.578	1.66	31.9	1.50	24.0	2.70	1.20
Ni	6.25	5.84	8.31	6.29	20.5	8.23	9.81	8.63
Cu	3.26	3.46	8.09	17.8	5.85	4.14	18.1	4.91
Zn	5.57	4.88	2.45	7.25	12.6	7.93	3.95	3.73
As	1.18	0.705	1.21	1.17	1.46	1.09	2.32	0.912
Rare-earth elements (ppm)								
La	6.49	5.02	6.21	6.55	5.16	6.33	6.64	2.34
Ce	13.7	10.7	13.7	15.4	10.5	13.9	30.3	14.5
Pr	1.41	1.07	1.32	1.49	1.11	1.40	1.67	0.526
Nd	5.12	3.88	4.82	5.46	4.17	5.05	6.67	2.01
Sm	0.963	0.677	0.894	1.03	0.801	0.915	1.47	0.422
Eu	0.312	0.204	0.308	0.343	0.249	0.278	0.454	0.149
Gd	0.769	0.484	0.679	0.844	0.696	0.703	1.3	0.401
Tb	0.123	0.072	0.105	0.127	0.115	0.092	0.186	0.066
Dy	0.814	0.427	0.682	0.725	0.73	0.569	1.13	0.443
Ho	0.179	0.076	0.14	0.149	0.146	0.113	0.232	0.096
Y	4.84	2.62	3.68	4.08	4.87	3.05	6.81	2.62
Er	0.55	0.205	0.428	0.425	0.412	0.30	0.683	0.30
Yb	0.614	0.16	0.446	0.412	0.347	0.244	0.668	0.334
Lu	0.092	0.022	0.066	0.060	0.052	0.036	0.101	0.049
Selected element ratios								
Zr/Hf	37.8	42.9	33.1	44.6	44.4	39.8	44.8	40.0
Ti/Zr	10.6	14.6	12.3	15.3	17.8	15.5	14.6	13.8
Th/Sc	1.61	2.74	2.74	1.21	0.59	1.57	0.48	1.28

may result from heterogeneous alteration at the source, as well as during erosion, transport and diagenesis. Even though the detrital microcline grains in the clastic fraction may suggest a contribution from a plutonic source, their almost Na-free composition is more consistent with a low-temperature metasomatic origin. Moreover, the lack of abundant or large detrital quartz grains is consistent with a dacitic rather than a granitic source. On the other hand, additional sources are needed to explain other particles such as the oxide-coated grains, micaceous clots and primary microclines in the detrital fraction.

Thus, the detrital fraction in Kromberg turbidites best represents a contribution from different sources, probably a mixture of previously metasomatized Hooggenoeg dacites and dacitic volcaniclastics, and another source that remains to be identified.

9. Model for chert formation

Each turbidite unit of the Kromberg Formation contains an almost complete Bouma sequence, as illustrated in Fig. 3. In modern Bouma sequences, the final member consists of clays or muds (Bouma, 1962), and this has led previous authors to argue that the cherty upper zone observed in the Kromberg Formation is the product of silicification of fine-grained volcaniclastic debris by secondary Si-rich fluids (e.g. Lowe and Knauth, 1977; Lowe, 1999; Rouchon et al., 2009). However, in the previous section, we show that in situ alteration of Kromberg volcaniclastics is restricted to partial alteration of K-feldspar to phyllosilicate minerals during diagenesis, as described by Rouchon and Orberger (2008) and Rouchon et al. (2009), perhaps augmented by low temperature

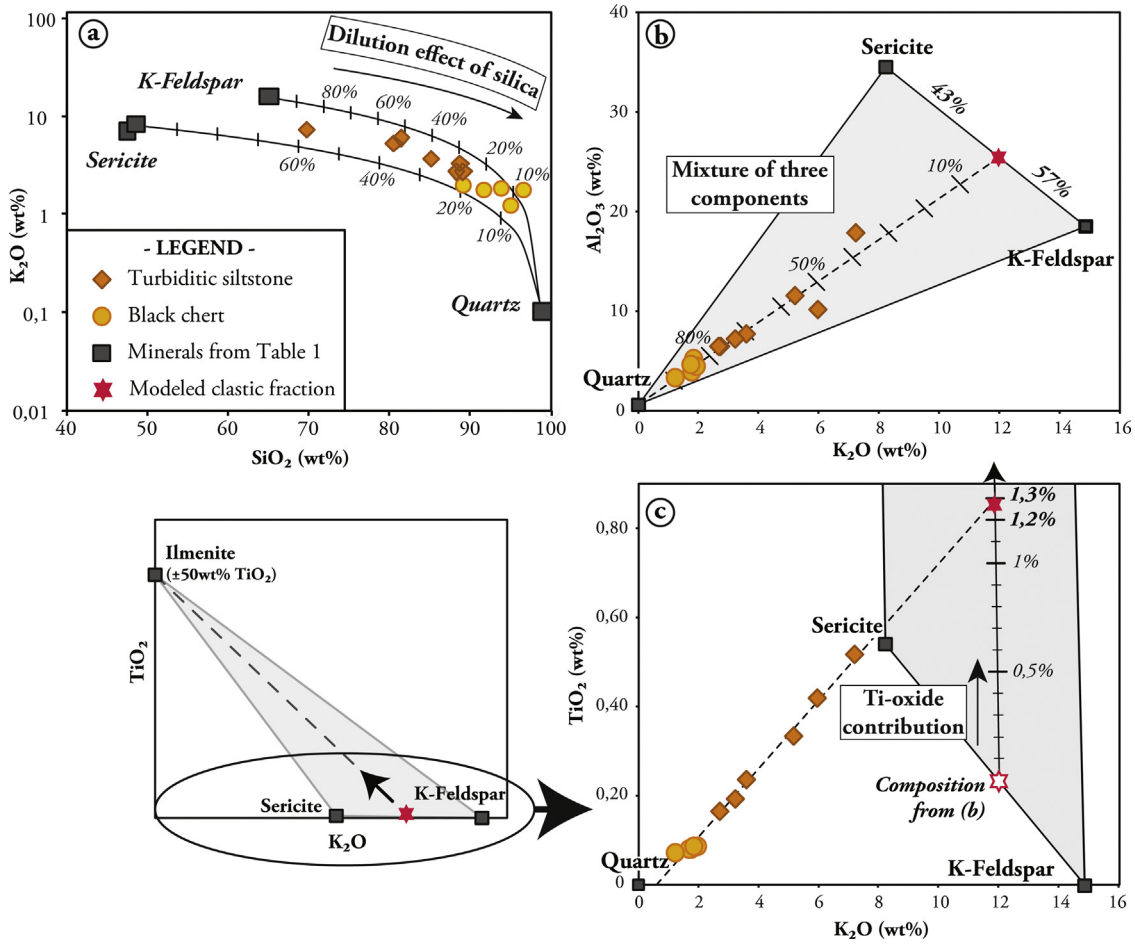

Fig. 13. Selected major element vs. major element diagrams showing (a) a decrease in potassium content with increasing silica concentrations, (b) a composition consistent with a three component mixing, i.e. K-feldspar and phyllosilicates in roughly equal proportions and an additional siliceous component that acts as a diluent, (c) a deviation of the expected composition due to the presence of ~1% of ilmenite.

hydrothermal silicification as suggested by Hofmann and Harris (2008).

Rouchon and Orberger (2008) proposed a model for chert formation in turbidites based on their study of dacite-derived, silicified silt- and sandstones from the Kitty's Gap locality, in Pilbara, Australia (<3446 ± 5 Ma; De Vries et al., 2006). These rocks strongly resemble and are nearly contemporaneous to Kromberg Fm. cherts (>3432 Ma; Grosch et al., 2011). The authors advocate the sorption of dissolved silica onto detrital particles as they settled through the water column and sedimented at the seafloor. Early diagenetic processes involved the infiltration of volcaniclastic debris by warm (>70 °C) and acid (pH 5.5–6.5) Archean seawater. The subsequent seritization of silicates to mica released additional silica, leading to the progressive cementation and induration of the sediment. Rouchon et al. (2009) applied this model to the Kromberg Fm. cherts and argued that fine clay particles or lithic fragments were more susceptible to silicification than coarser grains (e.g. feldspar) because of their higher sorption capacity. The differential silicification of fine- and coarse-grained sediments allowed higher porosity to remain in the sand-rich fraction, favoring fluid trapping and subsequent carbonatation in the lower parts of turbidites during the final stages of diagenesis (Rouchon et al., 2009).

Here, we propose new petrographic arguments that reinforce this model applied to the Kromberg siltstones and cherts. First of all, Rouchon et al. (2009) defined the Kromberg cherts as "replacement" cherts because "the sedimentary matrix is composed dominantly of microcrystalline quartz with minor sericite". They propose the following definition after Rouchon and Orberger (2008): "diagenetic precipitates of pure silica in bedding-parallel or crosscutting veins". They also insist on that these cherts are not chemically precipitated sedimentary rocks (e.g. Lowe, 1999; Tice and Lowe, 2006). However, although we agree with their model, we consider the terminology inappropriate as it implies a silicification during diagenesis whereas it already starts in the water column and during sedimentation. Instead, we prefer the term "chemico-clastic sediments", which best reflect the formation of the uppermost Bouma divisions by the chemical precipitation of marine silica triggered by the sedimentation of detrital particles. As emphasized by Rouchon and Orberger (2008) and Rouchon et al. (2009), such model rests on the capacity of clay to adsorb a significant amount of silica during their settling through the water column and at the sediment-seawater interface (e.g. Rimstidt and Barnes, 1980; Williams et al., 1985; Williams and Crerar, 1985).

After metasomatism and erosion of the dacitic source, the detrital feldspars, phyllosilicates and lithic fragments were transported to the basin and deposited by turbidity currents. As the turbiditic cloud settled, the detrital components were deposited according to their density, size and shape. This resulted in the deposition first of coarse fragments, then sand and silt, and finally, in our model, of clay and adsorbed silica. Numerous authors described how clay particles act as nuclei that trigger the flocculation of dissolved silica (e.g. Siever and Woodford, 1973; Williams et al., 1985; Williams and Crerar, 1985; Gehlen and Van Raaphorst, 2002; Grenne and Slack, 2003). This sorption process is controlled by the nature, settling velocity and specific area of the reactive particles and by the dissolved silica concentration, cation content, and pH of the solution.

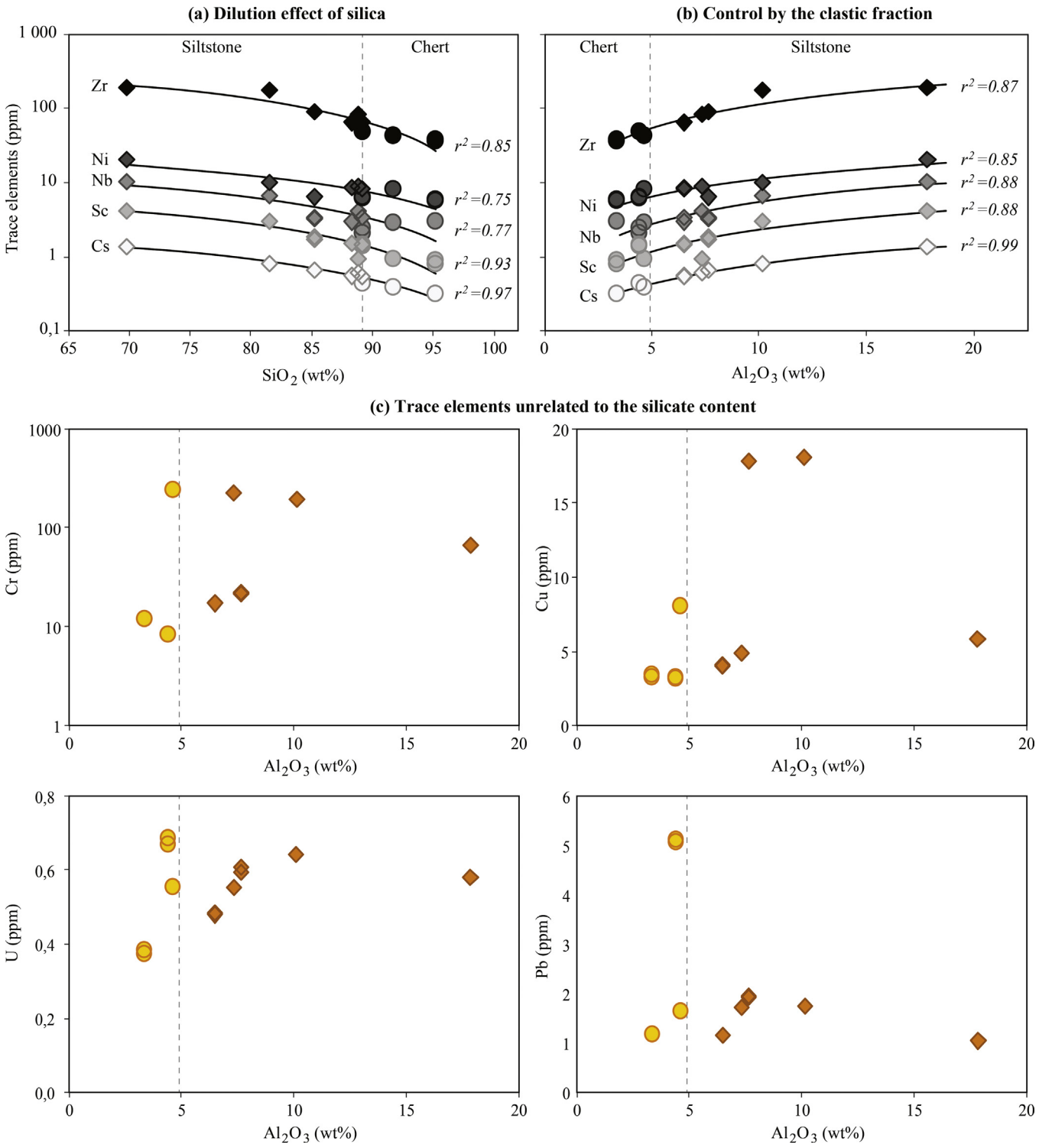

Fig. 14. Selected trace element vs. major element diagrams. (a) Decreasing trace element concentrations with increasing SiO_2 showing the sensitivity of trace elements to the dilution effect of silica. (b) Aluminum is used to represent the clastic fraction. The positive correlations with the trace elements demonstrate their location in the detrital grains (i.e. K-feldspars and K-micas). (c) Trace elements that lack correlations are either located in other phases unrelated to the aluminum content (e.g. carbonates), or were disturbed during secondary processes such as erosion, transport, diagenesis and metamorphism.

Accordingly, the low silica content in the coarser part of turbidites and its upward increasing is best explained (1) by the higher sorption capacity of clay minerals, (2) their higher surface-to-volume ratio and (3) by their low settling velocity at the end of deposition from turbidity currents (typically <0.1 mm/s for silt-size particles; Gibbs et al., 1971). Rouchon et al. (2009) calculated that 1 g of shale takes up about 35 mmol of silica whereas coarser sediments such as fine pebble conglomerates take up only 4.5 mmol. The sorption takes place either at the seawater–sediment interface or directly in the water column during particle settling.

The discontinuous clastic inputs from turbidity currents are thus considered responsible for the local and episodic precipitation of silica at Komati River. During turbidite emplacement, large amounts of suspended particles are rapidly introduced to the basin

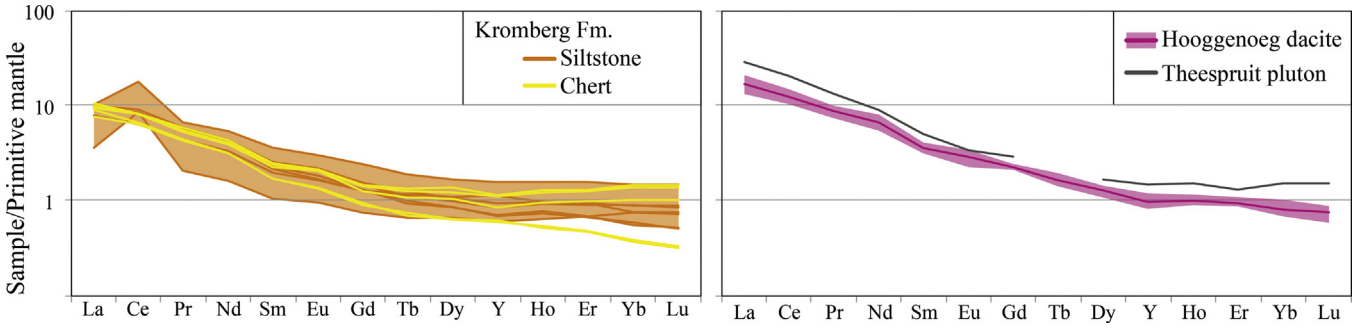

Fig. 15. Mantle-normalized (McDonough and Sun, 1995) rare earth element patterns of Kromberg chert and siltstone (left), Hooggeneog dacites (Rouchon et al., 2009) and Theespruit pluton (Abraham, 2010) (right). All the spectra have similar shapes with strongly fractionated patterns.

(Fig. 17) and trigger the heterogeneous nucleation of silica and the formation of silica flocs in the water column (Fig. 17-1 and 17-2). The growth, settling and accumulation of such aggregates first accompanied, then displaced the deposition of detrital grains to produce a siliceous gel at the top of Bouma sequences (Fig. 17-2). We envisage a colloidal layer in which silica flocs were uniformly mixed with very fine-grained particles. The silica flocs must have been cohesiveless and friable, like particles in modern volcanic lakes (e.g. Delmelle et al., 2000), so that they could be reworked by current action, as demonstrated by the ripple marks of Fig. 4b.

The formation of flame structures at the tops of chert horizons (Fig. 4c) suggests that the ooze behaved like mud at or just below the seabed (Oliveira et al., 2011; see also Oliveira et al., 2009). The structures resemble load-induced, antiformal sedimentary structures generally seen in fine- grained sediments such as mud and shales (e.g. Mills, 1983; Maltman and Bolton, 2003; Oliveira et al., 2011). They are produced by differential loading and vertical compression induced by the rapid sedimentation of a denser material onto a still-soft and water-rich substratum (McKee and Goldberg, 1969; Bishop, 1977). The presence of similar structures in the siliceous mud that later was transformed into the Kromberg cherts indicates that it was able to deform during the vertical compression and shear stress induced by successive turbidite deposits. Such rheological behavior is characteristic of thixotropic fluids such as colloidal suspensions of clay, mud and silica (Ambrose and Loomis, 1933; Perret et al., 1996; Barnes, 1997; Pignon et al., 1998; Besq et al., 2000; Coussot et al., 2002; Labanda and Llorens, 2006).

Following deposition, the sediments underwent diagenesis associated with (1) the precipitation of several generations of carbonates in the coarser part of turbidites (Rouchon et al., 2009) and (2) the rapid lithification of cherty tops to form impermeable caps of chert. The pore space in the uppermost layers of siltstone was progressively filled by precipitation of silica from pore water, which was seawater at first, then low-temperature, diagenetic fluids when the porosity network became gradually isolated from surface fluids. Such rapid and early induration of silica deposits at the Archean seafloor, already observed in other localities by Lowe (1999), can account for the rapid fossilization of the detrital fraction and its protection from subsequent in situ alteration.

Across the whole turbiditic section of Kromberg Fm., macro- and microscale evidence for high-temperature, hydrothermal fluid circulation, such as chert-filled concordant veins, cross-cutting fractures, and silicification fronts, is rare or absent, even in the coarser basal part of turbidites. The diagenetic conditions remained low-grade, as supported by the limited extent of seritization, weak development of silica embayments and lack of high-grade

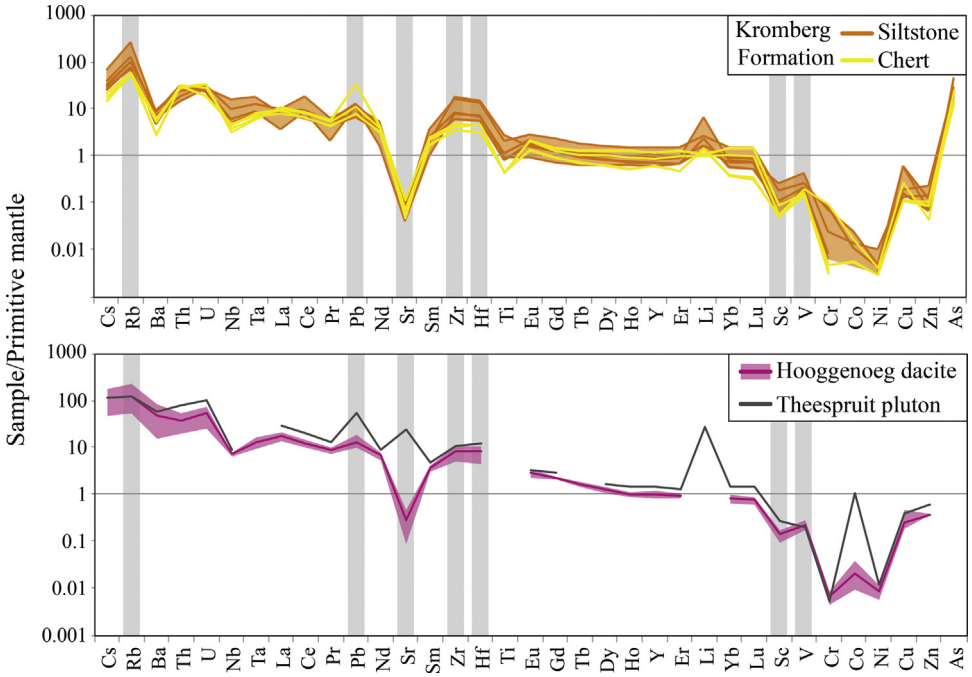

Fig. 16. Mantle-normalized (McDonough and Sun, 1995) trace-element patterns of Kromberg chert and siltstone (top), Hooggeneog dacites (Rouchon et al., 2009) and Theespruit pluton (Abraham, 2010) (right) (bottom).

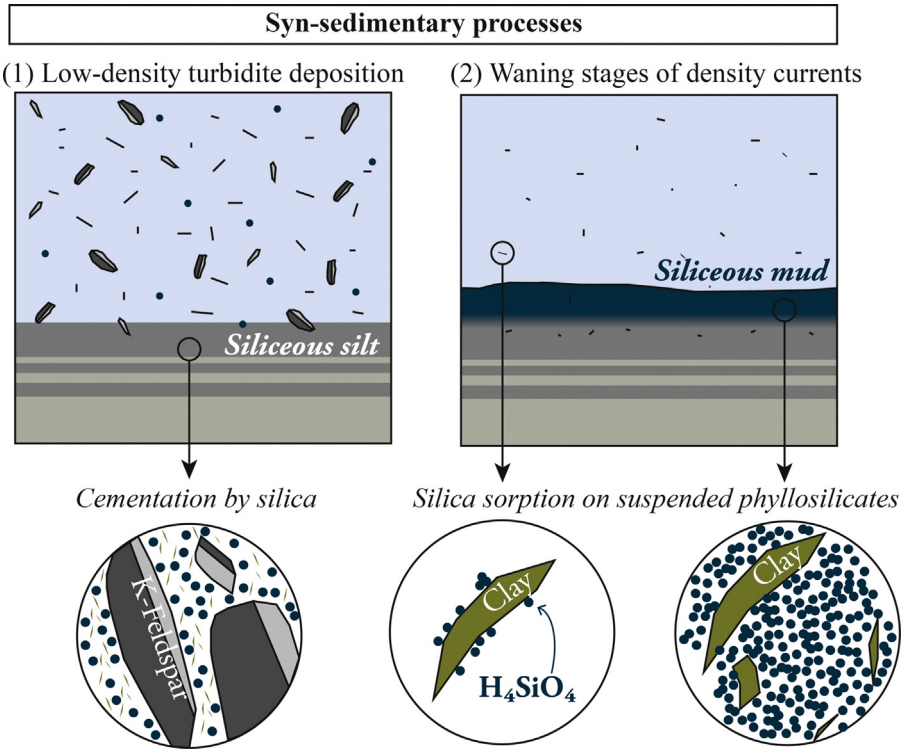

Fig. 17. Model for the formation of Kromberg chert. (1) The coarse and medium-grained fractions were deposited as siltstone near the top of Bouma sequences. (2) During the waning stage of clastic sedimentation, suspended clay serves as nuclei for silica flocculation. A siliceous ooze forms at the seafloor as the silica flocs grow and settle through the water column.

metasomatic crystal overgrowths. The final stage of sediment evolution was low-grade metamorphism that affected the whole Barberton Greenstone Belt (e.g. Grosch et al., 2012).

Our model may apply to most cherts deposited together with fine-grained detrital particles, such as tuffs and pyroclastic rocks (e.g. Stiegler et al., 2008, 2010). However, the precipitation of oceanic silica does not always require the presence of such particles. As an example, black and white banded chert sequences, such as the Buck Reef Chert of the Barberton belt (e.g. Tice and Lowe, 2006), and the homogeneous chert layers at the top of some komatiitic flows (e.g. Byerly, 1999) lack a clastic component. In these cases, other processes account for the precipitation of silica at the Archean seafloor.

10. Conclusion

The clastic deposits from the Kromberg type section, Barberton Greenstone Belt, contain dacitic volcaniclastics deposited by turbidity currents at the Archean seafloor. The upper members of Bouma sequences comprise homogeneous black chert horizons overlying Si-rich laminated siltstones. We argue that (1) the clastic particles are of detrital origin, (2) some of these particles were altered and metasomatized at source and (3) in situ metasomatism was limited to further seritization.

Using petrographic arguments, we reinforce the model of Rouchon and Orberger (2008) and Rouchon et al. (2009) whereby the siltstones formed by the deposition of clastic grains from turbidity currents followed by precipitation of silica on phyllosilicate grains, both in the water column and at the sediment–water interface. The clastic particles were derived mainly from the dacitic volcanics that stratigraphically underlie the cherts from the Kromberg section.

The evolution from silica-cemented siltstone to homogeneous chert is continuous through the top of the Archean Bouma sequence: as the rate of clastic sedimentation declined, the accumulation of silica flocs onto suspended phyllosilicates first accompanied, then replaced the deposition of detrital grains. The chert, which contained more than 85% of silica and less than 15% of fine-grained particles, thus was deposited as chemico-clastic sediment during this waning stage of turbidite deposition. It resulted in the formation of a siliceous ooze at the seafloor that behaved like modern, thixotropic muds. Our results favor a model in which clastic sedimentation serves as trigger mechanism for C-chert formation. Such a process may have prevailed in a variety of Archean setting where fine-grained sediments were deposited.

The composition of both the siltstone and chert reflects mainly the environment in which they formed. They can be interpreted as a mixture of two main components: (1) silica, which contains extremely low concentrations of trace elements and contributes only SiO_2 to the bulk composition, and (2) another phase that dominates the trace element composition. In Kromberg deposits, the second component is detrital K-feldspar, mica and a very minor amount of a Ti-phase (probably ilmenite), zircon and other heavy minerals. Accordingly, clastic-contaminated cherts are useful for classic sedimentology, such as provenance studies,

Acknowledgement

We acknowledge the EPOV program (CNRS) and the ANR project BEGDy (BLAN-0109) for their financial contribution to the project. The manuscript has been improved following discussions with Donald Lowe, Frances Westall and Christoph Heubeck. We thank Gordon Chunnett and Axel Hofmann for their contribution on the field, Anne-Marie Boullier for thin section interpretations, and also for the help in the lab at ISTerre we thank Sarah Bureau, Christelle Poggi and Catherine Chauvel for geochemical analyses, Nathaniel Findling for X-ray diffraction, Manuel Munoz for X-ray microfluorescence and Valentina Sobolev for microprobe analyses.

Appendix A. Supplementary data

Supplementary material related to this article can be found, in the online version, at http://dx.doi.org/10.1016/j.precamres.2014.10.009.

References

Abraham, K., (PhD thesis) 2010. Variation of stable isotopes: analytical developments and applications in Precambrian geochemistry. Johannes Gutenberg-Universität.

Alt, J., Teagle, D.A.H., 2003. Hydrothermal alteration of upper oceanic crust formed at a fast-spreading ridge: mineral, chemical, and isotopic evidence from ODP Site 801. Chem. Geol. 201 (3–4), 191–211.

Altermann, W., Kazmierczak, J., 2003. Archean microfossils: a reappraisal of early life on Earth. Res. Microbiol. 154, 611–617.

Ambrose, H.A., Loomis, A.G., 1933. Fluidities of thixotropic gels: bentonite suspensions. Physics 4 (8), 265.

Armstrong, R.A., Compston, W., de Wit, M.J., Williams, I.S., 1990. The stratigraphy of the 3.5–3.2 Ga Barberton greenstone belt revisited: a single zircon microprobe study. Earth Planet. Sci. Lett. 101 (1), 90–106.

Barnes, H.A., 1997. Thixotropy – a review. J. Non-Newtonian Fluid Mech. 70, 1–33.

Bau, M., Dulski, P., 1996. Distribution of yttrium and rare-earth elements in the Penge and Kuruman iron-formations, Transvaal Supergroup, South Africa. Precambrian Res. 79 (1–2), 37–55.

Bau, M., Möller, P., 1993. Rare earth element systematics of the chemically precipitated component in early Precambrian iron formations and the evolution of terrestrial atmosphere–hydrosphere–lithosphere system. Geochim. Cosmochim. Acta 57, 2239–2249.

Behnia, P., Collins, L.G., Samani, B.A., 2003. K- and Si-metasomatism, mineral transformation and formation of granitoids from basic rocks in Qooshchi area, NW Iran; A mineralogical Context. J. China Univ. Geosci. 14 (1), 34–41.

Behnia, P., Darvishzadeh, A., Collins, L.G., 2004. Geochemical peculiarities in K- and Si-metasomatic processes of Qooshchi Complex, Northwest Iran. Iran. Int. J. Sci. 5 (1), 77–90.

Besq, A., Monnet, P., Pantet, A., 2000. Flow situations of drilling muds – effects of thixotropicproperty. Flucome Euro.

Biggin, A.J., De Wit, M.J., Langereis, C.G., Zegers, T.E., Voûte, S., Dekkers, M.J., Drost, K., 2011. Palaeomagnetism of Archaean rocks of the Onverwacht Group, Barberton Greenstone Belt (southern Africa): evidence for a stable and potentially reversing geomagnetic field at ca. 3.5 Ga. Earth Planet. Sci. Lett. 303, 314–328.

Bishop, R.S., 1977. Shale diapir emplacement in south texas: Laward and Sherriff examples. Gulf Coast Assoc. Geol. Soc. Trans. 27, 20–31.

Bolhar, R., Kamber, B.S., Moorbath, S., Fedo, C.M., Whitehouse, M.J., 2004. Characterization of early Archaean chemical sediments by trace element signatures. Earth Planet. Sci. Lett. 222, 43–60.

Bolhar, R., Van Kranendonk, M.J., Kamber, B.S., 2005. A trace element study of siderite-jasper banded iron formation in the 3.45 Ga Warrawoona Group, Pilbara Craton – Formation from hydrothermal fluids and shallow water. Precambrian Res. 137, 93–114.

Bouma, A.H., 1962. Sedimentology of some Flysch deposits. A graphic approach to facies interpretation. Elsevier.

Brandl, G., Cloete, M., Anaeusser, C.R., 2006. Archaean greenstone belts. In: Johnson, M.R., Anhaeusser, C.R., Thomas, R.J. (Eds.), The Geology of South Africa. Geological Society of South Africa Johannesburg/Council for Geosciences, Pretoria, pp. 9–15.

Byerly, G., 1999. Komatiites of the Mendon formation: late-stage ultramafic volcanism in the Barberton Greenstone Belt. In: Lowe, D.R., Byerly, G.R. (Eds.), Geologic Evolution of the Barberton Greenstone Belt, vol. 329. Geological Society of America Special Papers, South Africa, pp. 189–212.

Chapin, C.E., Lindley, J.I., 1985. Potassium metasomatism of volcanic and sedimentary rocks in rift basins, calderas, and detachment terranes. In: Abstracts presented to "Terrestrial Planets: Comparative Planetology". California Institute of Technology, Pasadena, pp. 25.

Chauvel, C., Bureau, S., Poggi, C., 2011. Comprehensive chemical and isotopic analyses of basalt and sediment reference materials. Geostand. Geoanal. Res. 35 (1), 125–143.

Condie, K.C., 1993. Chemical composition and evolution of the upper continental crust: contrasting results from surface samples and shales. Chem. Geol. 104 (1–4), 1–37.

Coussot, P., Nguyen, Q.D., Huynh, H.T., Bonn, D., 2002. Viscosity bifurcation in thixotropic, yielding fluids. J. Rheol. 46 (3), 573.

De Vries, S.T., 2004. Early Archaean sedimentary basins: depositional environment and hydrothermal systems. Geol. Ultraiectina 244, 1–160.

De Vries, S.T., Nijman, W., Armstrong, R.A., 2006. Growth-fault structure and stratigraphic architecture of the Buck Ridge volcano-sedimentary complex, upper Hooggenoeg Formation, Barberton Greenstone Belt, South Africa. Precambrian Res. 149, 77–98.

de Wit, M.J., Hart, R., 1993. Earth's earliest continental lithosphere, hydrothermal flux and crustal recycling. Lithos 30, 309–335.

de Wit, M.J., Armstrong, R.A., Hart, R.J., Wilson, A.H., 1987a. Felsic igneous rocks within the 3.3–3.5 Ga Barberton greenstone belt: High crustal level equivalents of the surrounding tonalite-trondhjemite terrain, emplaced during thrusting. Tectonics 6, 529–549.

de Wit, M.J., Hart, R.A., Hart, R.J., 1987b. The Jamestown ophiolite complex, Barberton mountain belt; a section through 3.5 Ga oceanic crust. J. Afr. Earth Sci. 6, 681–730.

de Wit, M.J., Furnes, H., Robins, B., 2011. Geology and tectonostratigraphy of the onverwacht suite. Precambrian Res. 186 (1–4), 1–27.

de Wit, M.J., Hart, R.J., Martin, A., Abbott, P., 1982. Archaean abiogenic and probable biogenic structures associated with mineralized hydrothermal vent systems and regional metasomatism, with implications for greenstone belt studies. Econ. Geol. 77, 1783–1802.

Delmelle, P., Bernard, A., Kusakabe, M., Fischer, T.P., Takano, B., 2000. Geochemistry of the magmatic-hydrothermal system of Kawah Ijen volcano, East Java, Indonesia. J. Volcanol. Geother. Res. 97, 31–53.

Derry, L.A., Jacobsen, S.B., 1990. The chemical evolution of Precambrian seawater: evidence from REEs in banded iron formations. Geochim. Cosmochim. Acta 54 (11), 2965–2977.

Duchac, K.C., Hanor, J.S., 1987. Origin and timing of the metasomatic silicification of an early archean komatiite sequence, barberton mountain land, South Africa. Precambrian Res. 37 (2), 125–146.

Folk, R.L., 1980. Petrology of Sedimentary Rocks. Hemphill Austin, Texas.

Frei, R., Polat, A., 2007. Source heterogeneity for the major components of 3.7 Ga Banded Iron Formations (Isua Greenstone Belt, Western Greenland): Tracing the nature of interacting water masses in BIF formation. Earth Planet. Sci. Lett. 253 (1–2), 266–281.

Furnes, H., De Wit, M.J., Robins, B., Sandståd, N.R., 2011. Volcanic evolution of the upper Onverwacht Suite, Barberton Greenstone Belt, South Africa. Precambrian Res. 186, 28–50.

Garçon, M., Chauvel, C., Bureau, S., 2011. Beach placer, a proxy for the average Nd and Hf isotopic composition of a continental area. Chem. Geol. 287, 182–192.

Gehlen, M., Van Raaphorst, W., 2002. The role of adsorption–desorption surface reactions in controlling interstitial Si(OH)(4) concentrations and enhancing Si(OH)(4) turn-over in shallow shelf seas. Contin. Shelf Res. 22 (10), 1529–1547.

Gibbs, R.J., Meathews, M.D., Link, D.A., 1971. The relationship between sphere size and settling velocity. J. Sedim. Petrol. 41, 7–18.

Grenne, T., Slack, J.F., 2003. Paleozoic and mesozoic silica-rich seawater: evidence from hematitic chert (jasper) deposits. Geology 31 (4), 319–322.

Grosch, E.G., Kosler, J., McLoughing, N., Drost, K., Slama, J., Pedersen, R.B., 2011. Paleoarchean detrital zircon ages from the earliest tectonic basin in the Barberton Greenstone Belt, Kaapvaal craton, South Africa. Precambrian Res. 191 (1–2), 85–99.

Grosch, E.G., Vidal, O., Abu-Alam, T., McLoughlin, N., 2012. P-T constraints on the metamorphic evolution of the paleoarchean Kromberg type-section, Barberton Greenstone Belt, South Africa. J. Petrol. 53 (3), 513–545.

Hesse, R., 1989. Silica diagenesis: origin of inorganic and replacement cherts. Earth-Sci. Rev. 26 (C), 253–284.

Heubeck, C., Lowe, D.R., 1994. Depositional and tectonic setting of the Archean Moodies Group, Barberton Greenstone Belt, South Africa. Precambrian Res. 68 (3–4), 257–290.

Heubeck, C., Engelhardt, J., Byerly, G.R., Zeh, A., Sell, B., Luber, T., Lowe, D.R., 2013. Timing of deposition and deformation of the Moodies Group (Barberton Greenstone Belt, South Africa): Very-high-resolution of Archaean surface processes. Precambrian Res. 231, 236–262.

Hofmann, A., Bolhar, R., 2007. Carbonaceous cherts in the Barberton Greenstone Belt and their significance for the study of early life in the Archean record. Astrobiology 7, 355–388.

Hofmann, A., Harris, C., 2008. Silica alteration zones in the Barberton greenstone belt: A window into subseafloor processes 3.5–3.3 Ga ago. Chem. Geol. 257 (3–4), 221–239.

Hofmann, A., Wilson, A.H., 2007. Silicified basalts, bedded cherts and other sea floor alteration phenomena of the 3.4 Ga Nondweni greenstone belt, South Africa. In: Van Kranendonk, M.J., Smithies, R.H., Bennett, V. (Eds.), Earth's Oldest Rocks, vol. 15. Developments in Precambrian Geology, pp. 571–605.

Hofmann, A., 2005. The geochemistry of sedimentary rocks from the Fig Tree Group. Barberton greenstone belt: Implications for tectonic, hydrothermal and surface processes during mid- Archaean times. Precambrian Res. 143 (1–4), 23–49.

Jaffres, J.B.D., Shields, G., Wallman, K., 2007. The oxygen isotope evolution of seawater: a critical review of a long-standing controversy and an improved geological water cycle model for the past 3.4 billion years. Earth-Sci. Rev. 83, 83–122.

Kamo, S.L., Davis, D.W., 1994. Reassessment of Archean crustal development in the Barberton Mountain Land, South Africa, based on U-Pb dating. Tectonics 13 (1), 167–192.

Kastner, M., 1971. Authigenic feldspars in carbonate rocks. Am. Mineralosgist 56, 1403–1442.

Kato, Y., Nakamura, K., 2003. Origin and global tectonic significance of early Archean cherts from the Marble Bar greenstone belt, Pilbara Craton, Western Australia. Precambrian Res. 125, 191–243.

Knauth, L.P., Lowe, D.R., 1978. Oxygen isotope geochemistry of cherts from the Onverwacht Group (3.4 billion years), Transvaal, South Africa, with implications for secular variations in the isotopic composition of cherts. Earth Planet. Sci. Lett. 41 (2), 209–222.

Knauth, L.P., Lowe, D.R., 2003. High Archean climatic temperature inferred from oxygen isotope geochemistry of cherts in the 3.5 Ga Swaziland Supergroup, South Africa. Geol. Soc. Am. Bull. 115 (5), 566–580.

Knauth, L.P., (PhD Thesis) 1973. Oxygen and hydrogen isotope ratios in cherts and related rocks. Californian Institute of Technology, pp. 369.

Knauth, L.P., 1994. Petrogenesis of chert. In: Silica: physical behavior. geochemistry and materials applications. Rev. Mineral. 29, 233–258.

Kröner, A., Byerly, G., Lowe, D.R., 1991. Chronology of early Archean granite-greenstone evolution in the Barberton Mountain Land, South Africa, based on precise dating by signle zircon evaporation. Earth Planet. Sci. Lett. 103 (1–4), 41–54.
Labanda, J., Llorens, J., 2006. A structural model for thixotropy of colloidal dispersions. Rheol. Acta 45 (3), 305–314.
Lowe, D.R., Byerly, G.R., 1999. Stratigraphy of the west-central part of the Barberton Greenstone Belt, South Africa. In: Lowe, D.R., Byerly, G.R. (Eds.), Geologic evolution of the Barberton Greenstone Belt, South Africa. Geological Society of America Special Paper 329, 1–37.
Lowe, D.R., Fisher Worrell, G., 1999. Sedimentology, mineralogy, and implications of silicified evaporites in the Kromberg Formation, Barbeton Greenstone Belt, South Africa. In: Lowe, D.R., Byerly, G.R. (Eds.), Geological evolution of the Barberton Greenstone Belt, South Africa. Geological Society of America Special Paper 329, 167–188.
Lowe, D.R., Knauth, L.P., 1977. Sedimentology of the Onverwacht Group (3.4 billion years), Transvaal, South Africa, and its bearing on the characteristics and evolution of the early earth. J. Geol. 85 (6), 699–723.
Lowe, D.R., 1980. Archean sedimentation. Annu. Rev. Earth Planet. Sci. 8, 145–167.
Lowe, D.R., 1999. Petrology and sedimentology of cherts and related silicified sedimentary rocks in the Swaziland Supergroup. In: Lowe, D.R., Byerly, G.R. (Eds.), Geological evolution of the Barberton Greenstone Belt, South Africa. Geol. Soc. Am. Special Paper 329, 83–114.
Maliva, R.G., Knoll, A.H., Simonson, B.M., 2005. Secular change in the Precambrian silica cycle: Insights from chert petrology. Geol. Soc. Am. Bull. 117 (7/8), 835–845.
Maltman, A.J., Bolton, A., 2003. How sediments become mobilized. Geol. Soc. London Special Publication 216, 9–20.
Marin, J., Chaussidon, M., Robert, F., 2010. Microscale oxygen isotope variations in 1.9 Ga Gunflint cherts: assessments of diagenesis effects and implications for oceanic paleotemperature reconstructions. Geochim. Cosmochim. Acta 74 (1), 116–130.
Marin-Carbonne, J., Chaussidon, M., Boiron, M.-C., Robert, F., 2011. A combined in situ oxygen, silicon isotopic and fluid inclusion study of a chert sample from Onverwacht Group (3.35Ga, South Africa): new constraints on fluid circulation. Chem. Geol. 286 (3–4), 59–71.
Marin-Carbonne, J., Chaussidon, M., Robert, F., 2012. Micrometer-scale chemical and isotopic criteria (O and Si) on the origin and history of Precambrian cherts: Implications for paleo-temperature reconstructions. Geochim. Cosmochim. Acta 92, 129–147.
McDonough, W.F., Sun, S.-s., 1995. The composition of the Earth. Chem. Geol. 120, 223–253.
McKee, E.D., Goldberg, M., 1969. Experiments on formation of contorted structures in mud. Geol. Soc. Am. Bull. 80 (2), 231–244.
Mills, P.C., 1983. Genesis and diagnostic value of soft-sediment deformation structures—a review. Sedim. Geol. 35, 83–104.
Nothdurft, G.E., Webb, G.E., Kamber, B.S., 2004. Rare earth element geochemistry of Late Devonian reefal carbonates, Canning basin, Western Australia: confirmation of a seawater REE proxy in ancient limestones. Geochim. Cosmochim. Acta 68, 263–283.
Oliveira, C.M., Hodgson, D.M., Flint, S.S., 2009. Aseismic controls on in situ softsediment deformation processes and products in submarine slope deposits of the Karoo Basin, South Africa. Sedimentology 56, 1201–1225.
Oliveira, C.M., Hodgson, D.M., Flint, S.S., 2011. Distribution of soft-sediment deformation structures in clinoform successions of the Permian Ecca Group, Karoo Basin, South Africa. Sedim. Geol. 235, 314–330.
Orberger, B., Rouchoun, V., Westall, F., de Vries, S.T., Pinti, D.L., Wagner, C., Wirth, R., Hashizume, K., 2006. Micro-facies and the origin of some Archean Cherts (Pilbara, Australia). Geol. Soc. Am. Special Paper 405, 133–156.
Pack, A., Russell, S., Shelley, J., Michael, G., van Zuilen, M.A., 2007. Geo- and cosmochemistry of the twin elements yttrium and holmium. Geochim. Cosmochim. Acta 71 (18), 4592–4608.
Paris, I., Stanistreet, I.G., Hughes, M.J., 1985. Cherts of the Barberton Greenstone Belt Interpreted as Products of Submarine Exhalative Activity. J. Geol. 93 (2), 111–129.
Perret, A., Locat, P., Martignoni, P., 1996. Thixotropic behavior during shear of a fine-grained mud from Eastern Canada. Eng. Geol. 43 (1), 31–44.
Perry, E.C., Lefticariu, L., 2003. Formation and geochemistry of Precambrian cherts. Treatise Geochem. 7, 99–113.
Perry, E.C., Lefticariu, L., 2006. The oxygen isotopic composition of Precambrian cherts. Geochim. Cosmochim. Acta 70 (18), A483.
Pignon, F., Magnin, A., Piau, J.-M., 1998. Thixotropic behavior of clay dispersions: combinations of scattering and rheometric techniques. J. Rheol. 42 (6), 1349–1373.
Rimstidt, J.D., Barnes, H.L., 1980. The kinetics of silica–water interaction. Geochim. Cosmochim. Acta 44, 1683–1699.
Robert, F., Chaussidon, M., 2006. A palaeotemperature curve for the Precambrian oceans based on silicon isotopes in cherts. Nature 443 (7114), 969–972.
Rouchon, V., Orberger, B., 2008. Origin and mechanisms of K–Si-metasomatism of ca. 3.4-3.3 Ga volcaniclastic deposits and implications for Archean seawater evolution: Examples from cherts of Kittys Gap (Pilbara craton, Australia) and Msauli (Barberton Greenstone Belt, South Africa). Precambrian Res. 165 (3–4), 169–189.
Rouchon, V., Orberger, B., Hofmann, A., Pinti, D.L., 2009. Diagenetic Fecarbonates in Paleoarchean felsic sedimentary rocks (Hooggenoeg Formation, Barberton greenstone belt, South Africa): implications for CO_2 sequestration and the chemical budget of seawater. Precambrian Res. 172 (3–4), 255–278.
Schopf, J.W., Packer, B.M., 1987. Early Archean (3.3-billion to 3.5-billion-year-old) microfossils from Warrawoona Group, Australia. Science 237, 70–73.
Shields, G., Stille, P., 2001. Diagenetic constraints on the use of cerium anomalies as palaeoseawater redox proxies: an isotopic and REE study of Cambrian phosphorites. Chem. Geol. 175 (1–2), 29–48.
Shields, G.A., Webb, G.E., 2004. Has the REE composition of seawater changed over geological time? Chem. Geol. 204 (1–2), 103–107.
Siever, R., Woodford, N., 1973. Sorption of silica by clay minerals. Geochim. Cosmochim. Acta 37, 1851–1880.
Siever, R., 1992. The silica cycle in the Precambrian. Geochim. Cosmochim. Acta 56 (8), 3265–3272.
Stiegler, M.T., Lowe, D., Byerly, G.B., 2008. Abundant pyroclastic komatiitic volcanism in the 3.5-3.2 Ga Barberton Greenstone Belt, South Africa. Geol. Soc. Am. 36 (10), 779–782.
Stiegler, M.T., Lowe, D., Byerly, G.B., 2010. The petrogenesis of volcaniclastic komatiites in the Barberton Greenstone Belt, South Africa: a textural and geochemical study. J. Petrol. 51 (4), 947–972.
Sugitani, K., Horiuchi, Y., Adachi, M., Sugisaki, R., 1996. Anomalously low Al_2O_3/TiO_2 values for Archean cherts from the Pilbara Block, Western Australia - possible evidence for extensive chemical weathering on the early earth. Precambrian Res. 80, 49–76.
Sugitani, K., Yamamoto, K., Adachi, M., Kawabe, I., Sugisaki, R., 1998. Archean cherts derived from chemical, biogenic and clastic sedimentation in a shallow restricted basin: examples from the Gorge Creek Group in the Pilbara Block. Sedimentology 45 (6), 1045–1062.
Sugitani, K., 1992. Geochemical characteristics of Archean cherts and other sedimentary rocks in the Pilbara Block, Western Australia: Evidence for Archean seawater enriched in hydrothermally derived iron and silica. Precambrian Res. 57, 21–47.
Tice, M.M., Lowe, D.R., 2004. Photosynthetic microbial mats in the 3,416-Myrold ocean. Nature 431 (7008), 549–552.
Tice, M.M., Lowe, D.R., 2006. The origin of carbonaceous matter in pre-3.0 Ga greenstone terrains: A review and new evidence from the 3.42 Ga Buck Reef Chert. Earth-Sci. Rev. 76 (3/4), 259–300.
Treguer, P., Nelson, D.M., Van Bennekom, A.J., DeMaster, D.J., Leynaert, A., Queguiner, B., 1995. The silica balance in the world ocean: a reestimate. Science 268, 375–379.
Tucker, M.E., 1991. Sedimentary petrology: An introduction to the origin of sedimentary rocks, second ed. Wiley and Sons.
Ulrich, M., 2010. Péridotites et serpentinites du complexe ophiolitique de la Nouvelle-Calédonie. PhD manuscript;. Université de la Nouvelle-Calédonie et Université Joseph Fourier de Grenoble, pp. 1–272.
Van den Boorn, S., van Bergen, M.J., Nijman, W., Vroon, P.Z., 2007. Dual role of seawater and hydrothermal fluids in Early Archean chert formation: evidence from silicon isotopes. Geol. Soc. Am. 35 (10), 939–942.
Van den Boorn, S., van Bergen, M.J., Vroon, P.Z., de Vries, S.T., Nijman, W., 2010. Silicon isotope and trace element constraints on the origin of 3.5 Ga cherts: implications for early Archaean marine environments. Geochim. Cosmochim. Acta 74 (3), 1077–1103.
Van Kranendonk, M.J., Pirajno, F., 2004. Geochemistry of metabasalts and hydrothermal alteration zones associated with c. 3.45 Ga chert and barite deposits: implication for the geological setting of the Warrawoona Group, Pilbara Craton, Australia. Geochem. Expl. Env. Anal. 4, 253–278.
Van Kranendonk, M.J., Webb, G.E., Kamber, B.S., 2003. Geological and trace element evidence for a marine sedimentary environment of deposition and biogenicity of 3.45 Ga stromatolitic carbonates in the Pilbara Craton, and support for a reducing Archaean ocean. Geobiology 1 (2), 91–108.
Viljoen, M.J., Viljoen, R.P., 1969a. An introduction to the geology of the Barberton, granite-greenstone terrain. Geol. Soc. South Africa Special Publication 9, 1–20.
Viljoen, M.J., Viljoen, R.P., 1969b. The geology and geochemistry of the lower ultramafic unit of the Onverwacht Group and a proposed new class of igneous rocks. Geol. Soc. South Africa Special Publication 2, 55–86.
Walsh, M.M., 1992. Microfossils and possible microfossils from the Early Archean Onverwacht Group, Barberton Mountain Land, South Africa. Precambrian Res. 54, 271–292.
Webb, G.E., Kamber, B.S., 2000. Rare earth elements in Holocene reefal microbialites: a shallow seawater proxy. Geochim. Cosmochim. Acta 64, 1557–1565.
Weis, D., Wasserburg, G.J., 1987. Rb–Sr and Sm–Nd isotope geochemistry of cherts from the Onverwacht Group (3.5 AE), South Africa. Geochim. Cosmochim. Acta 51, 973–984.
Westall, F., de Wit, M.J., Dann, J., et al., 2001. Early Archean fossil bacteria and biofilms in hydrothermally- influenced sediments from the Barberton Greenstone belt, South Africa. Precambrian Res. 106, 93–116.
Williams, L.A., Crerar, D.A., 1985. Silica diagenesis; II, General mechanisms. J. Sedim. Res. 55 (3), 312–321.
Williams, L.A., Parks, G.A., Crerar, D.A., 1985. Silica diagenesis, I. Solubility controls. J. Sedim. Petrol. 55, 301–311.